Strobl, M., Hetzel, R., Niedermann, S., Ding, L., Zhang, L. (2012): Landscape evolution of a bedrock peneplain on the southern Tibetan Plateau revealed by in situ-produced cosmogenic 10Be and 21Ne. - Geomorphology, 153-154, 192-204

DOI: 10.1016/j.geomorph.2012.02.024

Landscape evolution of a bedrock peneplain on the southern Tibetan Plateau revealed by *in situ*-produced cosmogenic ^{10}Be and ^{21}Ne

M. Strobl [a,*], R. Hetzel [a], S. Niedermann [b], L. Ding [c], L. Zhang [c]

[a] Institut für Geologie und Paläontologie, Westfälische Wilhelms-Universität Münster, Corrensstr. 24, D-48149 Münster, Germany

[b] Helmholtz-Zentrum Potsdam – Deutsches GeoForschungsZentrum (GFZ), Telegrafenberg, D-14473 Potsdam, Germany

[c] Key Laboratory of Continental Collision and Plateau Uplift, Institute of Tibetan Plateau Research, Chinese Academy of Sciences, Beijing 100085, People's Republic of China

* Corresponding author: Marcus Strobl, Institut für Geologie und Paläontologie, Westfälische Wilhelms-Universität Münster, Corrensstr. 24, D-48149 Münster, Germany, Phone: +49 251 8333960, Fax: +49 251 9333968, E-mail address: marcus.strobl@uni-muenster.de.

Abstract

Low-relief bedrock surfaces that occur at high altitude are a common feature of Cenozoic mountain belts and have often been used to infer a significant amount of rock uplift after their generation at low elevation. The timescale over which such surfaces can be preserved at high elevation and the rate at which they are modified by weathering and erosion are poorly known. Here we use cosmogenic ^{10}Be and ^{21}Ne to quantify the landscape evolution of a bedrock peneplain in southern Tibet that occurs at an altitude of ~5300 m. The peneplain is developed in Cretaceous granitoids and Jurassic metasediments of the northern Lhasa block (90°E, 31°N) and originally had a minimum extent of ~150 km east-west and ~75 km north-south. It has been dissected by small rivers that generated a few hundred meters of relief and formed additional bedrock surfaces of limited extent at lower elevation. Local denudation rates for the peneplain and the lower bedrock surfaces – based on ^{10}Be concentrations in grus samples and amalgamated quartz clasts – cluster between 5 and 11 m Ma^{-1} (mean = 8.1 m Ma^{-1}) and are thought to be representative for the long-term rate of downwearing of these surfaces. Samples from bedrock outcrops and bedrock blocks yield more variable rates (3–20 m Ma^{-1}), which partly overestimate the long-term lowering rate, presumably due to block tilting and bedrock inhomogeneity. Spatially averaged ^{10}Be denudation rates for small river catchments range from 9 to 16 m Ma^{-1} (mean = 11.8 m Ma^{-1}) and are only slightly higher than the local denudation rates. Hence, the incision and widening of valleys proceeds at low rates, which demonstrates that the landscape of the peneplain region is remarkably stable. The combined ^{21}Ne and ^{10}Be data in a subset of the samples suggest that the bedrock surfaces have experienced a simple exposure history without periods of burial. Thus, our data do not provide any evidence for extended periods of shielding by ice during past glaciations, which is consistent with the absence of erratic boulders and moraines in the peneplain region.

Keywords: Tibet, peneplain, denudation rate, cosmogenic ^{10}Be, cosmogenic ^{21}Ne

1. Introduction

Low-relief surfaces eroded into bedrock have been documented in many mountain belts around the world, such as the Pyrenées (e.g. De Sitter, 1952), the Andes (e.g. Kennan et al., 1997; Hoke and Garzione, 2008), the Rocky Mountains (e.g. McMillan et al., 2006), the Gobi Altai (e.g. Jolivet et al., 2007), and the Himalaya (van der Beek et al., 2009). Typically, these bedrock surfaces occur at high altitudes of 2000 to 4000 m and are largely surrounded by areas with lower elevation that have steeper hillslopes. Hence, these low-relief surfaces are commonly interpreted as remnants of paleo-surfaces that had originally a much larger extent (e.g. De Sitter, 1952; Clark et al., 2005). Some workers have referred to these remnant surfaces as peneplains (e.g. Babault et al., 2005; Gunnell et al., 2009), a term that denotes a nearly featureless, gently undulating land surface of considerable area, which has been produced by subaerial erosion almost to base level (Jackson, 1997).

To what extent the paleo-surfaces that are present in many mountain belts have been uplifted after their formation remains a matter of debate. For instance, De Sitter (1952) argued that low-relief surfaces in the Pyrenées were formed near sea level and have subsequently been raised to an altitude of ~2000 m. In support of this view, Gunnell et al. (2009) presented biochronologic and thermochronologic data and suggested that the Eastern Pyrenées experienced a strong post-orogenic uplift by thermally driven thinning of the lithospheric mantle after 12 Ma. On the other hand, field observations and experimental data have been used to suggest that the low-relief surfaces in the Pyrenées were already formed at high elevation owing to the deposition of thick alluvial fans at the mountain front and a concomitant rise in base level (Babault et al., 2005, 2007). According to these authors, the erosive efficiency of the drainage network was reduced and surface planation took place at high altitude – an interpretation which raises doubts on the inference of a young post-tectonic uplift.

The Tibetan Plateau is the largest and highest plateau on Earth with a mean elevation of ~5000 m and a relief of less than 1 km at a wavelength of ~100 km (Fielding et al., 1994). The plateau consists of continental terranes that were successively accreted to the Asian continental margin before the collision of India with Asia (e.g. Dewey et al., 1988; Yin and Harrison, 2000; Tapponnier et al., 2001) (**Fig. 1**). The remarkably low relief of the Tibetan Plateau has been explained by the development of an internal drainage system and the progressive filling of intramontane basins by sediments eroded from the adjacent mountains (Métivier et al., 1998, Sobel et al., 2003; Liu-Zeng et al., 2008). Apart from the sediment-covered areas resulting from the process described above, older low-relief surfaces that are developed in bedrock have been documented in the southeastern Tibetan Plateau (Clark et al., 2004) and in the Lhasa terrane of southern Tibet (Strobl et al., 2010). In southeastern Tibet, the formation and subsequent uplift of a regional low-relief landscape was inferred from a reconstruction of the large-scale drainage system through time (Clark et al., 2004). The onset of uplift and accelerated erosion was constrained with low-temperature thermochronology at 9-13 Ma (Clark et al., 2005) and may be related to a southeast-directed flow of the lower crust (e.g. Royden et al., 1997; Schoenbohm et al., 2006). As a response to the induced surface uplift, major rivers such as the Yangtze and Mekong have deeply incised this part of the plateau (Clark et al., 2005) and their headward incision continues to diminish the internally

drained portion of the plateau (**Fig. 1**). In the Lhasa terrane, a well preserved bedrock peneplain occurs in the internally drained part of the plateau north of the lake Nam Co (Chinese: "Co" = lake) (Strobl et al., 2010) (**Figs. 1, 2**). Thermal modeling of low-temperature thermochronologic data indicates that this surface was formed just prior to the India-Asia collision and was uplifted from a low elevation during an early stage of the continental collision (Hetzel et al., 2011). A small data set of local and catchment-wide ^{10}Be denudation rates from the northwestern portion of the peneplain indicated that the peneplain is a rather stable geomorphic feature (Hetzel et al., 2011).

To date, most other studies that applied cosmogenic nuclides in the interior of the Tibetan Plateau have focused on exposure dating of moraines and erratic boulders (e.g. Schäfer et al., 2002; Owen et al., 2005; Chevalier et al., 2011 and references therein). Apart from the study mentioned above, only two other studies have hitherto inferred denudation rates using cosmogenic nuclides. The first ^{10}Be-based bedrock erosion rates were reported by Lal et al. (2003) for 17 samples distributed across entire Tibet. Most of these samples yielded erosion rates of 3 to 30 m Ma^{-1}, although high rates of up to 2000 m Ma^{-1} were obtained from a few samples in the Kunlun mountains in northern Tibet. Although the study by Lal et al. (2003) suggests that rates of bedrock erosion on the Tibetan Plateau are low, the limited geologic and geomorphic information provided on the studied sites precludes a detailed interpretation of their data. A second study in western Tibet (80°E, 35°N) focussed on mafic volcanic cones that contain quartz xenocrysts (Kong et al., 2007). The erosion rates inferred from ^{10}Be and ^{26}Al concentrations in ten quartz samples from these cones range from 4 to 24 m Ma^{-1} and support the view that bedrock is generally eroding at low rates. Interestingly, five of the investigated samples indicated a complex exposure history with significant periods of burial, which may result from a prolonged cover by ice or snow (Kong et al., 2007).

In this study, we present local and catchment-wide ^{10}Be denudation rates for a total of 53 samples that are distributed over the entire bedrock peneplain region north of Nam Co (**Fig. 2**). In addition, we combine ^{21}Ne and ^{10}Be concentrations measured in a subset of these samples to evaluate if the peneplain has experienced a simple exposure history with slow denudation only, or a complex exposure history that included periods of burial. Together with a detailed description of the geomorphology and bedrock geology the cosmogenic nuclide data set constrains the geomorphic evolution of the peneplain region.

2. Geological setting and characterization of the bedrock peneplain north of Nam Co

In the Nam Co region, the boundary between the internally and externally drained portions of the Tibetan Plateau extends along the crest of the Nyainqentanglha Shan (Chinese: "Shan" = mountain) and separates two regions with a markedly different topography signature (**Fig. 2**). The area southeast of the drainage divide, which comprises the headwater region of the Tsangpo river, the Yadong–Gulu rift, and the south-east facing slopes of the Nyainqentanglha Shan, has a rugged morphology with steep hillslopes and high local relief (Armijo et al., 1986; Strobl et al., 2010). The Nyainqentanglha Shan has been uplifted in the footwall of a low-angle normal fault that strikes ENE-WSW along the northern margin of the tectonically active Yadong-Gulu rift (Armijo et al., 1986; Pan and Kidd, 1992; Harrison et al., 1995). In contrast, the region north of the Nyainqentanglha Shan belongs to the internally drained part of the plateau and is characterized by a subdued morphology with low local relief, many

lakes, and vast plains covered by alluvial sediment (**Fig. 2**). The climate in this region is cold and arid with a mean annual temperature of 0°C and an annual precipitation of ~300 mm (Daut et al., 2010; Mügler et al., 2010).

The area north of Nam Co is dominated by remnants of a vast bedrock peneplain, which extends for ~150 km east-west and ~75 km north-south (Strobl et al., 2010). The active N-S trending Bam Co graben subdivides this region into a western and an eastern part (**Fig. 2**). The eastern part is bounded to the north by an active right-lateral strike-slip fault, which has formed a pull-apart basin occupied by lake Bong Co (Armijo et al., 1989). Apart from these structures, no evidence for active deformation has been observed. The well preserved remnants of the bedrock peneplain occur at altitudes between 5200 m and 5400 m with a mean of ~5300 m. The lack of tectonic activity suggests that the different peneplain remnants were originally part of a more extensive surface. Today, these different parts are separated by small valleys with rivers that transport sediment to the broad, sediment-covered plains which mainly occur at an elevation of 4600-4700 m (**Figs. 2, 3a**). Hillslopes are largely covered by a thin mantle of regolith with local exposures of bedrock. Field observations and the analysis of digital elevation models in the northwestern part of the peneplain near the town Bangoin (**Fig. 3a**) revealed that hillslope angles increase toward lower elevation, which indicates that the peneplain is the oldest landscape element and was later dissected by the streams. The progressive incision of these streams has generated additional bedrock surfaces of limited extent below the main peneplain surface (Strobl et al., 2010).

The bedrock in the peneplain region consists of Cretaceous granitoids with U-Pb zircon ages of 110-120 Ma (Xu et al., 1985; Harris et al., 1988; Hetzel et al., 2011) that intruded very low-grade metamorphic Jurassic sediments (mainly siltstones and sandstones), and Lower Cretaceous sediments and volcanic rocks (Leeder et al., 1988) (**Fig. 3b**). The planar peneplain remnants occur predominantly in the granitoids and the resistant Jurassic metasediments (**Figs. 3b, 4a**) and do not follow a specific stratigraphic boundary. Originally, the peneplain may have also been present in the Cretaceous sediments, however, owing to the low strength of these sedimentary rocks it was not preserved there. An exception is an area located northeast of Nam Co with predominantly Cretaceous volcanic rocks (**Fig. 3b**).

On the flat peneplain remnants and the smaller surfaces that were formed during progressive river incision, the bedrock is either exposed or covered by block fields (**Fig. 4b**). The soil between the blocks appears to be thin and contains large amounts of granite grus. Flat bedrock outcrops are commonly dissected by polygonal fractures filled with grus and soil (**Fig. 4c**). During progressive disintegration by freezing and thawing such bedrock exposures may be transformed to block fields (e.g. Ives, 1958; Ballantyne, 1998), which typically consist of blocks with a size of a few decimeters up to about two meters (**Fig. 4d**). In the entire peneplain region we did not detect any erratic boulders, moraines, or glacially sculpted bedrock surfaces. Hence, Quaternary glaciations seem to have left no clear imprint on the geomorphology, although it cannot be ruled out that cold-based ice had accumulated on the flat surfaces during glacial periods in the past. We will address this question when discussing the exposure history with two-nuclide plots based on cosmogenic ^{10}Be and ^{21}Ne.

3. Sampling and analytical procedures

3.1 Sampling strategy

In order to test what kind of samples are best suited to quantify local denudation rates that are representative at the outcrop scale, we used four different sample types: samples from bedrock outcrops (n=10) and bedrock blocks (n=3), amalgamated quartz clasts (n=4), and grus samples (n=22) (**Table 1**). All these samples were taken either from the main peneplain or from flat surfaces at lower elevation (**Fig. 4a, b**). For the bedrock samples we chose sites where soil cover is minimal and mainly restricted to bedrock fractures (**Fig. 4c**) or is completely absent. Two samples (08T5 and –T6) were taken from meter-sized bedrock highs about six meters apart that stick out of the flat surrounding bedrock. Sample 08T5 is from the horizontal top of a bedrock high that has several ~15-cm-deep weathering pits and is elevated 1.2 m above the adjacent bedrock. The second sample (08T6) is from a bedrock high with rounded edges that stands 0.4 m above the surrounding ground and lacks weathering pits. In regions where the bedrock is covered by block fields, we sampled three large blocks with a diameter of at least one meter that appeared to rest in a stable position in the surrounding soil and blocks underneath. The 2-m-long block where we took sample 08T11 (**Fig. 4d**) had 1-3 cm deep weathering pits that seemed to indicate that the block has remained in a stable position for a long period of time. In addition to the bedrock samples, we took samples consisting of amalgamated quartz clasts or granite grus over areas with a size of 10 to 400 m^2. For each quartz clast sample we collected at least a hundred clasts with a size of about one centimeter. The grus samples were sieved in the field to obtain the 0.25–2 mm size fraction. In order to quantify spatially integrated denudation rates for entire river catchments, we took 14 sediment samples from creeks or from sandbars in small rivers draining the peneplain region (**Table 2**). The respective catchments ranged in size from 2 to 53 km^2 (**Fig. 5**).

3.2 Beryllium separation and analysis

The bedrock, clast, and grus samples were first crushed and then all samples were washed and sieved. Subsequently, the 250–500 μm grain size fraction was split into a magnetic and a non-magnetic fraction using a Frantz magnetic separator. This was followed by one etching step in 6M HCl, several etching steps in diluted HF/HNO_3 in a heated ultrasonic bath (Kohl and Nishiizumi, 1992), and two alternating etching steps in aqua regia and 8M HF to obtain pure quartz. After addition of ~0.3 mg of Be-carrier, the quartz samples were dissolved, Be was separated by successive anion and cation exchange columns, and precipitated at pH 8-9 as $Be(OH)_2$. Following the transformation to BeO at 1000 °C and target preparation, ^{10}Be was analyzed at the accelerator mass spectrometer (AMS) facility of ETH Zurich (Kubik and Christl, 2010). The blank-corrected ^{10}Be concentrations reported in Tables 1 and 2 are normalized to the secondary ETH standard S2007N, which has a nominal $^{10}Be/^{9}Be$ ratio of 28.1×10^{-12} (Kubik and Christl, 2010) considering the ^{10}Be half-life of 1.387 Ma (Chmeleff et al., 2010; Korschinek et al., 2010). The secondary standard is in use since April 2010 and has been calibrated to the primary standard ICN 01-5-1 (Nishiizumi et al., 2007; Kubik and Christl, 2010).

It is noteworthy that the ICP-OES analysis of the chemically cleaned quartz samples revealed that eleven of the 53 quartz samples had natural Be concentrations between 0.1 and 1 ppm; one sample (08T5) even had a Be content of 1.6 ppm. Given the mass of purified

quartz that was dissolved per sample (~15 g), the natural ^{9}Be amounts to a few percent of the Be that was added with the Be carrier solution (the largest value was 7.4% for sample 08T5). All samples with elevated Be contents were analyzed twice using ICP-OES and the natural Be concentrations were taken into account when calculating the concentrations of *in situ*-produced cosmogenic ^{10}Be.

3.3 Neon analysis and data reduction

Apart from ^{10}Be, we also analyzed the neon isotopic composition of a subset of seven quartz samples in the noble gas laboratory of the Deutsches GeoForschungsZentrum (GFZ) in Potsdam (**Table 3**). Before the analysis, the purified quartz samples were ground to a grain size of <100 μm to diminish the proportion of noble gases from fluid inclusions. Samples of ~0.7 g each were wrapped in Al-foil and placed in a sample carrousel under ultrahigh vacuum, where they were baked at 100°C for about one week to remove adsorbed atmospheric gases. Extraction of noble gases was achieved by stepwise heating at 400, 600, 800 and 1200 °C in an ultrahigh vacuum furnace. After removal of active gases in Ti sponge and ZrAl getters, the noble gases were trapped in a cryogenic adsorber at 11 K and sequentially released for analysis in a VG5400 mass spectrometer. In addition, the isotopic composition of neon contained in fluid inclusions was checked by analyzing the gas released by crushing ~1.0 g samples of the 250-500 μm quartz fraction in vacuo. Three of the crushed samples (08T2, -16, -27) were subsequently used for stepwise heating, while separate aliquots were taken otherwise. All data have been corrected for mass discrimination effects, isobaric interferences, and analytical blanks. Error limits correspond to the 95% confidence level; they include statistical uncertainties of the measurement, uncertainties of sensitivity and mass discrimination determination, and blank and interference corrections. Further details about the analytical procedures and data reduction methods can be found in Niedermann et al. (1997) and Goethals et al. (2009a).

Cosmic-ray-produced Ne in quartz is characterized by a unique ^{22}Ne/^{21}Ne ratio and therefore mixtures of cosmogenic Ne and another Ne component must plot on the 'spallation line' in a three-isotope diagram (Niedermann et al., 1993). As the trapped Ne components released by the crushing procedure have ^{21}Ne/^{20}Ne ratios that slightly exceed the one of air (^{21}Ne/^{20}Ne = 0.00296), the cosmogenic ^{21}Ne concentration of each sample was determined from the excesses in the 400, 600, and 800 °C temperature steps relative to the crushing extraction values (cf. Hetzel et al., 2002) (**Table 3**). Above 800°C, no more cosmogenic Ne is released from quartz (Niedermann, 2002). Small to moderate amounts of excess ^{21}Ne released in the 1200°C steps are interpreted to be nucleogenic ^{21}Ne, which is supported by the positions of 1200°C data in the Ne three-isotope plots away from the 'spallation line' (Figure S1 of the Supplementary Information).

4. Results

4.1 Calculation of ^{10}Be denudation rates

Cosmogenic nuclides allow to quantify rates of denudation, because the nuclide concentration of a steadily eroding surface depends on the rate of erosion (Lal, 1991). Although the term erosion is often used to describe the removal of mass from the Earth´s surface, the cosmogenic nuclide concentrations also reflect the loss of mass owing to chemical

weathering. In other words, concentrations of cosmogenic nuclides record the sum of physical erosion and chemical weathering, which is collectively referred to as denudation (Riebe et al., 2003; von Blanckenburg, 2006). The ^{10}Be denudation rates reported in this study (**Tables 1, 2**) were obtained with the CRONUS-Earth online calculator (Balco et al., 2008), version 2.2 with version 2.2.1 of the constants file (http://hess.ess.washington.edu). For the various parameters, e.g. the effective attenuation length of neutrons or the contribution of muons to cosmogenic nuclide production, we used the default values of the online calculator if not mentioned otherwise. For determining catchment-wide denudation rates we took the mean elevation of the respective catchments to calculate the nuclide production rate and quantified the topographic shielding using the Matlab script of Greg Balco (http://depts.washington.edu/cosmolab/shielding.m) and a digital elevation model with a resolution of 30 m (**Table 2**). The topographic shielding of the samples that were used to determine local denudation rates was negligible. A potential shielding by snow or ice has not been taken into account.

In order to allow a direct comparison of our data with those of previous studies (Lal et al., 2003; Kong et al., 2007), we used the constant production rate scaling model of Lal (1991) – Stone (2000) in the online calculator. The local ^{10}Be denudation rates obtained from bedrock exposures and bedrock blocks vary from 2.7 to 20.2 m Ma^{-1}, whereas the amalgamated clast and grus samples cluster between 5.3 and 14.2 m Ma^{-1} (mean = 8.1 m Ma^{-1}) (**Fig. 6a, b**). The stream sediment samples yielded catchment-wide denudation rates ranging from 8.6 to 16.3 m Ma^{-1} (mean = 11.8 m Ma^{-1}) (**Fig. 6c**). The timescale over which denudation rates integrate is equivalent to the time required to remove about 60 cm of bedrock (Granger et al., 1996; von Blanckenburg, 2006) and is thus inversely correlated to the denudation rate. The integration times for our samples range from ~40 to ~230 ka (**Tables 1, 2**).

4.2 ^{10}Be – ^{21}Ne erosion island plot

To evaluate whether the peneplain region was covered by ice for a significant period of time in the past, we combined the ^{10}Be and ^{21}Ne concentrations that were obtained from seven samples and plotted them in an "erosion island" plot (cf. Lal, 1991) of ^{10}Be versus ^{21}Ne/^{10}Be (**Fig. 7**). The plot was generated with the software CosmoCalc (Vermeesch, 2007) and the values of the different parameters chosen in CosmoCalc are outlined in the caption of figure 7. Six out of seven data points are consistent with a simple exposure history. Only one sample, which was taken from a bedrock block, lies above the saturation line in the complex exposure history field. The implications of these results will be discussed in more detail in section 5.4.

5. Discussion

5.1 Comparison of denudation rates obtained from different sample types

In the Nam Co area of southern Tibet, local ^{10}Be denudation rates for a large-scale peneplain at ~5300 m altitude and smaller bedrock surfaces at lower elevation were obtained from four different kinds of samples. The denudation rates derived from granite grus and amalgamated quartz clasts range from ~5 to ~14 m Ma^{-1} and show much less scatter than those inferred from bedrock exposures and bedrock blocks, which range from ~3 to ~20 m Ma^{-1} (**Fig. 6a, b**).

As both the grus and clast samples – which were taken over areas of 10 to 400 m^2 – consist of many grains, their ^{10}Be concentrations average a large number of individual denudation histories. Therefore, the denudation rates from these samples are interpreted to be more representative than those derived from bedrock blocks and bedrock exposures (cf. Hancock and Kirwan, 2007; Meyer et al., 2010).

Two bedrock blocks from a block field in the northwestern part of the peneplain (**Fig. 4d**) yielded high apparent denudation rates of ~12.8 and ~20.2 m Ma^{-1}. We consider these denudation rates as unreasonably high, because two grus samples from the same sites and three additional grus samples in this portion of the peneplain show consistent denudation rates of ~6.4 to ~7.5 m Ma^{-1} (**Fig. 5a**). We attribute the high rates inferred from the bedrock blocks to be caused by frost heave and block tilting as a result of repeated freeze-and-thaw cycles (cf. Dahl, 1966; Ballantyne, 1998). We envision that the sampled block surfaces were partly shielded and thus experienced a time-integrated ^{10}Be production rate that is lower than the one for an exposed horizontal surface. This would have led to lower ^{10}Be concentrations and thus to high apparent denudation rates. Although the third bedrock block yielded a low denudation rate of 2.7 m Ma^{-1} (**Fig. 6a**), we conclude that sampling bedrock blocks from block fields carries the risk of significantly overestimating long-term denudation rates.

Most samples from bedrock exposures yielded denudation rates of 5 to 8 m Ma^{-1}, i.e. similar to those inferred from grus and quartz clast samples (**Fig. 6a, b**). At nearly all sites where both grus or clast samples and bedrock were analyzed, the resulting denudation rates are in good agreement (**Fig. 5a-c**). The two samples from adjacent bedrock highs that stand 1.2 and 0.4 m above the surrounding ground (08T5 and –T6), respectively, gave denudation rates that differ by a factor of two. The larger bedrock high, which had distinct weathering pits on the flat upper surface, yielded a denudation rate of ~7.9 m Ma^{-1}, whereas the sample from the lower surface without weathering pits yielded a rate of ~16.6 m Ma^{-1}. This shows that – at least at the outcrop scale – the variable development of weathering features reflects local differences in denudation rate. A bedrock and a grus sample (08T29 and –T30) from northwest of Bangoin yielded consistent but relatively high denudation rates of ~16.9 and ~14.2 m Ma^{-1}, respectively (**Fig. 5a**). The two latter samples are from a region that has a more irregular morphology and lacks well-developed flat surfaces. The rates obtained from these two samples suggest that this area, which is located below the peneplain, is indeed experiencing a more rapid denudation than most other parts of the study area – probably because the granitic bedrock here is less resistant to weathering and physical erosion. Finally we note that the three granitoid samples analyzed by Lal et al. (2003) yielded ^{10}Be denudation rates that range from ~3.3 to ~7.8 m Ma^{-1} and are thus similar to our results (the location of these three samples is shown in **Fig. 3b**).

The spatially integrated denudation rates inferred from stream sediment samples for 14 catchments cluster between 8.6 and 16.3 m Ma^{-1} with a mean of 11.8 m Ma^{-1} (**Fig. 6c**). These rates are thus slightly higher than the mean local denudation rate of ~8.1 m Ma^{-1} derived from the grus and quartz clast samples. This is expected because the catchments include portions with somewhat larger hillslope angles (albeit not steeper than 25-30°, Strobl et al., 2010) that are denuding more rapidly than the subhorizontal surfaces where we determined the local denudation rates. The rather small difference in the mean rates suggests that river incision and hillslope lowering proceed slowly and therefore the landscape of the peneplain region is

remarkably stable. Importantly, both local and catchment-wide denudation rates obtained in the three subregions (**Fig. 5a-c**) reveal no systematic spatial pattern, in particular no correlation with altitude.

5.2 Uncertainties of the ^{10}Be denudation rates

The derivation of local and catchment-wide denudation rates from cosmogenic nuclide concentrations is based on several assumptions that have been described and discussed in detail by others (e.g. Lal, 1991; Brown et al., 1995; Dunai, 2010). One of these assumptions is that denudation has been steady through time, so that cosmogenic nuclide concentrations have attained a secular equilibrium (Lal, 1991). During the Quaternary, however, the global climate has repeatedly shifted from glacial to interglacial conditions and these fluctuations may have led to changes in the rate of denudation. On the Tibetan Plateau, cold and dry conditions during marine isotope stage 2 were followed by a warm and humid period with high lake levels in the early-mid Holocene (e.g. Wang et al., 2002; Mügler et al., 2010). A subsequent phase of increased aridity, which started 5-6 ka ago, is documented by falling lake levels (e.g. Lister et al., 1991; Lee et al., 2009; Mügler et al., 2010). These past changes in temperature and moisture conditions result from a variable strength of the monsoon system (e.g. Thompson et al., 1997; Liu et al. 1998; Herzschuh, 2006) and may have caused changes in the rate of denudation through time. The effect of such changes in denudation rate on the present-day concentration of cosmogenic nuclides has been investigated by numerical models that allow to compare a synthetic input erosion history with the erosion rate that would be calculated from the nuclide concentration of a sample taken today (Bierman and Steig, 1996; Heimsath, 2006; von Blanckenburg, 2006). These models reveal that stepwise changes in the erosion rate between 5 and 10 m Ma^{-1} over 100 ka climate cycles are almost completely damped out (e.g. von Blanckenburg, 2006), because for landscapes eroding that slowly the integration timescale of cosmogenic nuclides is several tens of thousands of years (see **Tables 1, 2**). In other words, even if the rate of denudation in the peneplain region has varied by a factor of two during Quaternary climate changes, it is likely that the denudation rates determined in this study provide a representative long-term average that integrates over glacial-interglacial cycles.

Calculating denudation rates from *in situ*-produced cosmogenic nuclides in quartz implicitly assumes that the relatively insoluble mineral quartz is not enriched in the regolith by preferential dissolution of other minerals such as feldspar (Small et al., 1999). If quartz in the regolith has been enriched relative to the bedrock, then the calculated denudation rates are underestimated (Small et al., 1999; Riebe et al., 2001). By analyzing the immobile element zirconium in both bedrock and regolith in catchments with granitic lithologies, Riebe et al. (2001) showed that over a wide range of temperate climates, the bias introduced ranges from 1 to 12 %. We argue that under the cold and arid climate prevailing in southern Tibet, the preferential enrichment of quartz by chemical weathering is unlikely to exceed a few percent. Hence, the underestimation of the denudation rates owing to the possible enrichment of quartz in the grus samples and the stream sediments is presumably of minor importance for the local and catchment-wide denudation rates reported in this study.

In quantifying the denudation rates we did not account for a potential shielding by snow, which would decrease the production rate of ^{10}Be. In this respect the reported denudation

rates are therefore maximum values, although the shielding effect is presumably small given the low annual precipitation of only ~300 mm in the study area (Li et al., 2008; Daut et al., 2010). For instance, even if the entire annual precipitation would fall as snow and remain at the surface for six months per year, the local ^{10}Be production rates and therefore the real denudation rates would only decrease by ~4.5 %.

On the other hand, the production rates of cosmogenic nuclides during glacial periods were probably higher than during the Holocene on the Tibetan Plateau, because factors such as (1) atmospheric compression due to cooling and (2) changes in global atmospheric dynamics owing to the presence of polar ice sheets led to changes in air pressure (Staiger et al., 2007). As indicated by the application of a general circulation model, these changes are greatest at high elevations and on the Tibetan Plateau they have probably caused production rates during the last glacial maximum to be ~6% higher than today (Staiger et al., 2007). The time-integrated effect on the production rates over ~50 to ~150 ka is likely to be much smaller but difficult to quantify. As this climate effect has not been taken into account when applying the CRONUS-Earth online calculator, it will likely cause a slight underestimation of the inferred denudation rates.

Two other factors might introduce a bias in the inferred catchment-wide denudation rates: prolonged periods of sediment storage (e.g. Granger et al., 1996) and the occurrence of bedrock landslides in the valleys upstream of the sediment samples (e.g. Niemi et al., 2005). Field observations provide no evidence for either of these two processes. In support of this conclusion, we note that (1) the relief of the relatively small catchments (2 to 53 km^2) does not exceed a few hundred meters, (2) the valleys are small and have narrow valley bottoms that do not offer significant accommodation space for the storage of sediments, and (3) the hillslope angles adjacent to the small rivers are smaller than 25-30°.

As stated in section 4 we applied the constant production rate scaling model of Lal (1991) – Stone (2000) for quantifying the denudation rates with the CRONUS-Earth online calculator. It is important to note that the time-dependent scaling models, which attempt to account for secular variations of the geomagnetic field, lead to higher production rates and thus to higher denudation rates. At the high altitude of around 5000m on the Tibetan Plateau these differences are considerably more pronounced than at lower elevation. For the time-dependent adaptation of the Lal (1991) – Stone (2000) scaling model (cf. Balco et al., 2008) the difference is ~15%, whereas the scaling schemes of Dunai (2001), Desilets and Zreda (2003), Desilets et al. (2006), and Lifton et al. (2005) lead to denudation rates that are about 30 to 40% higher than those reported herein. The exact differences depend on, among other factors, the integration time and the sample elevation, because the altitude-dependence of nuclide production slightly differs in the various scaling models. In summary, the discussion above reveals that the most significant uncertainty associated with the ^{10}Be denudation rates of this study is the uncertainty introduced by the scaling model that is used to calculate the local nuclide production rates. This important point has also been highlighted by Owen et al. (2008) and Chevalier et al. (2011) and emphasizes the urgent need for a production rate calibration site at high elevation of ~5 km – ideally such a site should be located on the Tibetan Plateau.

5.3 Implications for sediment generation and deposition in the peneplain region

Although the local and catchment-wide denudation rates in the peneplain region are low, a significant volume of sediment must have been generated during progressive valley incision and lowering of the peneplain over millions of years. As the peneplain region belongs to the internally drained part of the plateau (**Fig. 1**), the sediment produced cannot leave the interior of the plateau. The occurrence of Miocene lacustrine strata suggests that numerous lakes in south and central Tibet existed already between 13 and 23 Ma (Wu et al., 2008). Hence, the internal drainage system has likely persisted since the Miocene. As the volume of sediments that are present in the small valleys of the peneplain region is insignificant, most of the sediment that has been produced in the past millions of years was either deposited on the broad floodplains or transported to lakes such as Bam Co and Bong Co, which are situated in actively subsiding basins bounded by normal or strike-slip faults (**Fig. 2**). Owing to its sheer size Nam Co may also contain significant volumes of sediment, although it remains unknown whether the inferred normal fault along its southeastern margin is active and the lake bottom experiences tectonic subsidence (Strobl et al., 2010).

5.4 Evaluating past burial of the peneplain by glaciers or cold-based ice

Moraines and U-shaped valleys on both sides of the Nyainqentanglha Shan (**Fig. 2**) indicate that during the last glacial cycle glaciers descended down to ~4800 m on the northern slope of the mountain range and to about 4300–4500 m on its southern margin (Lehmkuhl et al., 2002; Klinge and Lehmkuhl, 2004). In the southern part of the Nyainqentanglha Shan, boulders from a sequence of three moraines yielded ^{10}Be exposure ages of ~34 ka, ~25 ka, and ~12 ka (Chevalier et al., 2011; the exposure ages were calculated with the scaling scheme of Lifton et al., 2005). Five boulders from an even older moraine in the eastern part of the mountain range have minimum ^{10}Be ages between ~50 ka and ~110 ka and indicate a slightly larger ice extent during the penultimate glaciation (Owen et al., 2005). For the moraines on the northwestern side of the Nyainqentanglha Shan no exposure ages are available, however, geomorphologic observations and a few minimum luminescence ages on aeolian silt, which locally rests on top of the glacial deposits, indicate that two moraine ridges formed during the last glaciation, whereas an older moraine is related to the penultimate glaciation (Lehmkuhl et al., 2002; Klinge and Lehmkuhl, 2004).

The available information summarized above suggests that a former advance of glaciers from the Nyainqentanglha Shan to the peneplain is very unlikely and this is corroborated by the absence of erratic boulders and moraines in the area north of Nam Co. This inference, however, does not preclude the accumulation of cold-based ice in the peneplain region. For instance, flat summit surfaces in Labrador, Canada, were buried under non-erosive ice during past glaciations as revealed by erosion island plots based on cosmogenic ^{10}Be and ^{26}Al (Marquette et al., 2004). In our case, the combination of cosmogenic ^{10}Be and ^{21}Ne concentrations does not provide any evidence for significant periods of burial, because six out of seven samples have a nuclide inventory that is consistent with a simple exposure history (**Fig. 7**). Note that four of these six samples are bedrock samples, whereas two samples (08T17 and –27) consist of amalgamated quartz clasts. Sample 08T17 was taken at the same site as bedrock sample 08T16 and the nuclide inventory of both samples suggests a simple exposure history (**Fig. 7**). The only sample that plots into the complex exposure history field (08T9) and may indicate a phase of burial was taken from a bedrock block. As discussed in

section 5.1, however, this bedrock block yields an unreasonably high ^{10}Be denudation rate of ~12.8 m Ma^{-1} – presumably because it has been tilted by frost heave. Thus, we consider the apparently complex exposure history indicated by this sample as geologically meaningless. In summary, the combined analysis of ^{21}Ne and ^{10}Be in a subset of our samples indicates that at least during the past hundred thousand years no cold-based ice was present in the peneplain region north of Nam Co. This is not surprising, because the ~7000-m-high Nyainqentanglha Shan constitutes an efficient topographic barrier that has presumably blocked the monsoonal precipitation from the peneplain region during past glaciations (Owen et al., 2005). At a larger spatial scale, our data are also inconsistent with the postulated presence of a Late Pleistocene ice sheet on the Tibetan Plateau as envisaged by Kuhle (1998). The existence of such an ice sheet is also negated by exposure ages of up to ~170 ka, which were obtained from moraines in central Tibet (Schäfer et al., 2002).

6. Conclusions

The analysis of cosmogenic ^{10}Be in four different kinds of samples from a large-scale bedrock peneplain in southern Tibet indicates that grus and amalgamated quartz clasts are best-suited to infer geologically meaningful denudation rates at the outcrop scale. The mean denudation rate obtained from this sample type is ~8 m Ma^{-1}, whereas catchment-wide denudation rates for small watersheds derived from stream sediment are only slightly higher and range from 9–16 m Ma^{-1} (mean ~12 m Ma^{-1}). The small difference between the local and spatially integrated rates demonstrates that the relief production proceeds at low rates. Hence, the geomorphology of the peneplain region has been barely modified during the last few millions of years. In addition, the combined use of cosmogenic ^{10}Be and ^{21}Ne in a small sub-suite of samples indicates that the peneplain region experienced a simple exposure history without periods of burial underneath cold-based ice.

The denudation rates reported in this study are afflicted with several uncertainties that may result from the following processes: (1) temporal changes in the rate of denudation as a result of Quaternary climate fluctuations, (2) a potential enrichment of quartz in the regolith relative to the bedrock, (3) a lowering of the nuclide production rate owing to snow shielding, and (4) temporally increased production rates during glacial periods as a result of atmospheric compression and changes in atmospheric dynamics. The cumulative uncertainty of the ^{10}Be-based denudation rates related to these processes is likely smaller than 10%, because the different uncertainties partially cancel out. At the high altitude of the Tibetan Plateau the most significant uncertainty affecting ^{10}Be denudation rates is the uncertainty introduced by the choice of the scaling model, which is needed to calculate local nuclide production rates. As a consequence, a reliable calibration of the ^{10}Be production rate at the high elevation of the Tibetan Plateau would be highly desirable.

Acknowledgments

This study was funded by the German Research Foundation (DFG) within the framework of the Priority Programme No. 1372 (grants HE 1704/8-1 and –/8-2) and by the National Natural Science Foundation for Distinguished Young Scholars (grant 40625008 to Ding Lin), and supported by the Deutsches GeoForschungsZentrum (GFZ) Potsdam. We are grateful to Pieter Vermeesch (University College London) for discussions on two-nuclide plots and to

Peter Kubik (ETH Zurich) for the AMS measurements. Andreas Struffert is thanked for his help in preparing the samples and Enzio Schnabel for performing the noble gas analyses. The constructive reviews of two anonymous reviewers are greatly appreciated.

References

Armijo, R., Tapponnier, P., Mercier, J.L., Han, T.L., 1986. Quaternary extension in southern Tibet: field observations and tectonic implications. J. Geophys. Res. 91, 13803-13872.

Armijo, R., Tapponnier, P., Tonglin, H., 1989. Late Cenozoic right-lateral strike-slip faulting in Southern Tibet. J. Geophys. Res. 94, 2787-2838.

Babault, J., Van Den Driessche, J., Bonnet, S., Castelltort, S., Crave, A., 2005. Origin of the highly elevated Pyrenean peneplain. Tectonics 24, TC2010, doi:10.1029/2004TC001697.

Babault, J., Bonnet, S., Van Den Driessche, J., Crave, A., 2007. High elevation of low-relief surfaces in mountain belts: does it equate to post-orogenic surface uplift? Terra Nova 19, 272-277.

Balco, G., Stone, J.O., Lifton, N.A., Dunai, T.J., 2008. A complete and easily accessible means of calculating surface exposure ages or erosion rates from ^{10}Be and ^{26}Al measurements. Quat. Geochron. 3, 174-195.

Ballantyne, C.K., 1998. Age and significance of mountain-top detritus. Permafrost and Periglacial Processes 9, 327-345.

Bierman, P.R., Steig, E.J., 1996. Estimating rates of denudation using cosmogenic isotope abundances in sediment. Earth Surf. Proc. Landf. 21, 125-139.

Brown, E.T., Stallard, R.F., Larsen, M.C., Raisbeck, G.M., Yiou, F., 1995. Denudation rates determined from the accumulation of in situ-produced ^{10}Be in the Luquillo Experimental Forest, Puerto Rico. Earth Planet. Sci. Lett. 129, 193-202.

Chevalier, M.L., Hilley, G., Tapponnier, P., Van Der Woerd, J., Liu-Zeng, J., Finkel, R.C., Ryerson, F.J., Li, H., Liu, X., 2011. Constraints on the late Quaternary glaciations in Tibet from cosmogenic exposure ages of moraine surfaces. Quat. Sci. Rev. 30, 528-554.

Chmeleff, J., von Blanckenburg, F., Kossert, K., Jakob, D., 2010. Determination of the ^{10}Be half-life by multicollector ICP-MS and liquid scintillation counting. Nucl. Instr. Meth. Phys. Res. B 268, 192-199.

Clark, M.K., Schoenbohm, L.M., Royden, L.H., Whipple, K.X., Burchfiel, B.C., Zhang, X., Tang, W., Wang, E., Chen, L., 2004. Surface uplift, tectonics, and erosion of eastern Tibet from large-scale drainage patterns. Tectonics 23, TC1006, doi:10.1029/2002TC001402.

Clark, M.K., House, M.A., Royden, L.H., Whipple, K.X., Burchfiel, B.C., Zhang, X., Tang, W., 2005. Late Cenozoic uplift of southeastern Tibet. Geology 33, 525-528.

Dahl, R., 1966. Block fields, weathering pits and tor-like forms in the Narvik Mountains, Nordland, Norway. Geogr. Annaler 48A, 55-85.

Daut, G., Mäusbacher, R., Baade, J., Gleixner, G., Kroemer, E., Mügler, I., Wallner, J., Wang, J., Zhu, L., 2010. Late Quaternary hydrological changes inferred from lake level fluctuations of Nam Co (Tibetan Plateau, China). Quat. Int. 218, 86-93.

DeCelles, P.G., Robinson, D.M., Zandt, G., 2002. Implications of shortening in the Himalayan fold-thrust belt for uplift of the Tibetan Plateau. Tectonics 21, TC1062, doi:10.1029/2001TC001322.

Desilets, D., Zreda, M., 2003. Spatial and temporal distribution of secondary cosmic-ray

nucleon intensities and applications to in situ cosmogenic dating. Earth Planet. Sci. Lett. 206, 21-42.

Desilets, D., Zreda, M., Prabu, T., 2006. Extended scaling factors for in situ cosmogenic nuclides: New measurements at low latitude. Earth Planet. Sci. Lett. 246, 265-276.

De Sitter, L.U., 1952. Pliocene uplift of Tertiary mountain chains. Am. J. Sci. 250, 297-307.

Dewey, J.F., Shackleton, R.M., Chang, C.F., Sun, Y.Y., 1988. The tectonic evolution of the Tibetan Plateau. Phil. Trans. R. Soc. London Series A 327, 379-413.

Ding, L., Kapp, P., Zhong, D., Deng, W., 2003. Cenozoic volcanism in Tibet: evidence for a transition from oceanic to continental subduction. J. Petrol. 44, 1833-1865.

Dunai, T.J., 2001. Influence of secular variation of the geomagnetic field on production rates of in situ produced cosmogenic nuclides. Earth Planet. Sci. Lett. 193, 197-212.

Dunai, T.J., 2010. Cosmogenic nuclides – principles, concepts and applications in the Earth surface sciences, Cambridge University Press, 1st edition, 187 pages.

Fielding, E., Isacks, B., Barazangi, M., Duncan, C., 1994. How flat is Tibet? Geology 22, 163-167.

Goethals, M.M., Niedermann, S., Hetzel, R., Fenton, C.R., 2009a. Determining the impact of faulting on the rate of erosion in a low-relief landscape: A case study using *in situ* produced ^{21}Ne on active normal faults in the Bishop Tuff, California. Geomorphology 103, 401-413.

Goethals, M.M., Hetzel, R., Niedermann, S., Wittmann, H., Fenton, C.R., Kubik, P.W., Christl, M., von Blanckenburg, F., 2009b. An improved experimental determination of cosmogenic ^{10}Be/^{21}Ne and ^{26}Al/^{21}Ne production ratios in quartz. Earth Planet. Sci. Lett. 284, 187-198.

Granger, D.E., Kirchner, J.W., Finkel, R., 1996. Spatially averaged long-term erosion rates measured from in situ-produced cosmogenic nuclides in alluvial sediment. J. Geol. 104, 249-257.

Gunnell, Y., Calvet, M., Brichau, S., Carter, A., Aguilar, J.P., Zeyen, H., 2009. Low long-term erosion rates in high-energy mountain belts: Insights from thermo- and biochronology in the Eastern Pyrenees. Earth Planet. Sci. Lett. 278, 208-218.

Hancock, G., Kirwan, M., 2007. Summit erosion rates deduced from ^{10}Be: Implications for relief production in the central Appalachians. Geology 35, 89-92.

Harris, N.B.W., Xu, R.H., Lewis, C.L., Jin, C.W., 1988. Plutonic rocks of the 1985 Tibet geotraverse, Lhasa to Golmud. Phil. Trans. R. Soc. London A327, 145-168.

Harrison, T.M., Copeland, P., Kidd, W.S.F., Lovera, O.M., 1995. Activation of the Nyainqentanghla Shear Zone: Implications for uplift of the Southern Tibetan Plateau. Tectonics 14, 658-676.

Heimsath, A.M., 2006. Eroding the land: Steady state and stochastic rates and processes through a cosmogenic lens, in: Siame, L.L., Bourlès, D.L., Brown, E.T. (Eds.), In Situ–Produced Cosmogenic Nuclides and Quantification of Geological Processes, Geological Society of America Special Paper 415, Boulder, pp. 111-129.

Heisinger, B., Lal, D., Jull, A.J.T., Kubik, P., Ivy-Ochs, S., Knie, K., Nolte, E., 2002. Production of selected cosmogenic radionuclides by muons: 2. Capture of negative muons. Earth Planet. Sci. Lett. 200, 357-369.

Herzschuh, U., 2006. Palaeo-moisture evolution in monsoonal Central Asia during the last

50,000 years. Quat. Sci. Rev. 25, 163-178.

Hetzel, R., Niedermann, S., Ivy-Ochs, S., Kubik, P.W., Tao, M., Gao, B., 2002. ^{21}Ne versus ^{10}Be and ^{26}Al exposure ages of fluvial terraces: the influence of crustal Ne in quartz. Earth Planet. Sci. Lett. 201, 575-591.

Hetzel, R., Dunkl, I., Haider, V., Strobl, M., von Eynatten, H., Ding, L., Frei, D., 2011. Peneplain formation in southern Tibet predates India-Asia collision and plateau uplift. Geology 39, 983-986.

Hoke, G.D., Garzione, C.N., 2008. Paleosurfaces, paleoelevation, and the mechanisms for the late Miocene topographic development of the Altiplano plateau. Earth Planet. Sci. Lett. 271, 192-201.

Ives, J.D., 1958. Mountain-top detritus and the extent of the last glaciation in northeastern Labrador-Ungava. The Canadian Geographer 3, 25-31.

Jackson, J.A., 1997. Glossary of geology. American Geological Institute, Alexandria, Virginia, 4th edition, 769 p.

Jolivet, M., Ritz, J.F., Vassallo, R., Larroque, C., Braucher, R., Todbileg, M., Chauvet, A., Sue, C., Arnaud, N., De Vicente, R., Arzhanikova, A., Arzhanikov, S., 2007. Mongolian summits: An uplifted, flat, old but still preserved erosion surface. Geology 35, 871-874.

Kennan, L., Lamb, S.H., Hoke, L., 1997. High-altitude palaeosurfaces in the Bolivian Andes: evidence for late Cenozoic surface uplift. In: Widdowson, M. (Ed.), Paleosurfaces: Recognition, Reconstruction and Palaeoenvironmental Interpretation. Geol. Soc. London Spec. Publ., vol. 120, pp. 307-323.

Klinge, M., Lehmkuhl, F., 2004. Pleistocene glaciations in southern and eastern Tibet. In: Ehlers, J., Gibbard, P. L. (Eds.), Quaternary Glaciations – Extent and Chronology, Part III, Oxford, pp. 361-369.

Kohl, C.P., Nishiizumi, K., 1992. Chemical isolation of quartz for measurement of in-situ produced cosmogenic nuclides. Geochim. Cosmochim. Acta 56, 3583–3587.

Kong, P., Na, C., Fink, D., Ding, L., Huang, F., 2007. Erosion in northwest Tibet from *in-situ*-produced cosmogenic ^{10}Be and ^{26}Al in bedrock. Earth Surf. Proc. Landf. 32, 116-125.

Korschinek, G., Bergmaier, A., Faestermann, T., Gerstmann, U.C., Knie, K., Rugel, G., Wallner, A., Dillmann, I., Dollinger, G., von Gostomski, Ch.L., Kossert, K., Maiti, M., Poutivtsev, M., Remmert, A., 2010. A new value for the half-life of ^{10}Be by Heavy-Ion Elastic Recoil Detection and liquid scintillation counting. Nucl. Instr. Meth. Phys. Res. B 268, 187-191.

Kubik, P.W., Christl, M., 2010. ^{10}Be and ^{26}Al measurements at the Zurich 6 MV Tandem AMS facility. Nucl. Instr. Meth. Phys. Res. B 268, 880-883.

Kuhle, M., 1998. Reconstruction of the 2.3 million km^2 late Pleistocene ice sheet on the Tibetan Plateau and its impact on the global climate. Quat. Int. 45, 71-108.

Lal, D., 1991. Cosmic ray labeling of erosion surfaces: In situ nuclide production rates and erosion models. Earth Planet. Sci. Lett. 104, 424-439.

Lal, D., Harris, N.B.W., Sharma, K.K., Gu, Z., Ding, L., Liu, T., Dongal, W., Caffee, M.W., Jull, A.J.T., 2003. Erosion history of the Tibetan Plateau since the last interglacial: constraints from the first studies of cosmogenic ^{10}Be from Tibetan bedrock. Earth Planet. Sci. Lett. 217, 33-42.

Lee, J., Li, S.-H., Aitchison, J.C., 2009. OSL dating of paleoshorelines at Lagkor Tso, western

Tibet. Quat. Geochron. 4, 335-343.

Leeder, M.R., Smith, A.B., Jixiang, Y., 1988. Sedimentology, palaeoecology and palaeoenvironmental evolution of the 1985 Lhasa to Golmud geotraverse, Phil. Trans. R. Soc. London A327, 107-143.

Lehmkuhl, F., Klinge, M., Lang, A., 2002. Late Quaternary glacier advances, lake level fluctuations and aeolian sedimentation in Southern Tibet. Zeitschr. Geomorph. Suppl. Bd. 126, 183-218.

Li, M., Kang, S., Zhu, L., You, Q., Zhang, Q., Wang, J., 2008. Mineralogy and geochemistry of the Holocene lacustrine sediments in Nam Co, Tibet. Quat. Int. 187, 105-116.

Lifton, N.A., Bieber, J.W., Clem, J.M., Duldig, M.L., Evenson, P., Humble, J.E., Pyle, R., 2005. Addressing solar modulation and long-term uncertainties in scaling secondary cosmic rays for in situ cosmogenic nuclide applications. Earth Planet. Sci. Lett. 239, 140-161.

Lister, G.S., Kelts, K., Zao, C.K., Yu, J.-Q., Niessen, F., 1991. Lake Qinghai, China: closed-basin lake levels and the oxygen isotope record for ostracoda since the latest Pleistocene. Palaeogeogr. Palaeoclimatol. Palaeoecol. 84, 141-162.

Liu, K., Yao, Z., Thompson, L.G., 1998. A pollen record of Holocene climate changes from the Dunde ice cap, Qinghai-Tibetan Plateau. Geology 26, 135-138.

Liu-Zeng, J., Tapponnier, P., Gaudemer, Y., Ding, L., 2008. Quantifying landscape differences across the Tibetan plateau: Implications for topographic relief evolution. J. Geophys. Res. 113, F04018. doi:10.1029/2007JF000897.

Marquette, G.C., Gray, J.T., Gosse, J.C., Courchesne, F., Stockli, L., Macpherson, G., Finkel, R., 2004. Felsenmeer persistence under non-erosive ice in the Torngat and Kaumajet mountains, Quebec and Labrador, as determined by soil weathering and cosmogenic nuclide exposure dating. Can. J. Earth Sci. 41, 19-38.

McMillan, M.E., Heller, P.L., Wing, S.L., 2006. History and causes of post-Laramide relief in the Rocky Mountain orogenic plateau. Geol. Soc. Am. Bull. 118, 393-405.

Métivier, F., Gaudemer, Y., Tapponnier, P., Meyer, B., 1998. Northeastward growth of the Tibet plateau deduced from balanced reconstruction of two depositional areas: The Qaidam and Hexi Corridor basins, China. Tectonics 17, 823-842.

Meyer, H., Hetzel, R., Fügenschuh, B., Strauss, H., 2010. Determining the growth rate of topographic relief using in situ-produced ^{10}Be: A case study in the Black Forest, Germany. Earth Planet. Sci. Lett. 290, 391-402.

Mügler, I., Gleixner, G., Günther, F., Mäusbacher, R., Daut, G., Schütt, B., Berking, J., Schwalb, A., Schwark, L., Xu, B., Yao, T., Zhu, L., Yi, C., 2010. A multi-proxy approach to reconstruct hydrological changes and Holocene climate development of Nam Co, Central Tibet. J. Paleolimnol. 43, 625-648.

Niedermann, S., 2002. Cosmic-ray-produced noble gases in terrestrial rocks: Dating tools for surface processes. Rev. Min. Geochem. 47, 731-784.

Niedermann, S., Graf, Th., Marti, K., 1993. Mass spectrometric identification of cosmic-ray-produced neon in terrestrial rocks with multiple neon components. Earth Planet. Sci. Lett. 118, 65-73.

Niedermann, S., Bach, W., Erzinger, J., 1997. Noble gas evidence for a lower mantle component in MORBs from the southern East Pacific Rise: decoupling of helium and

neon isotope systematics. Geochim. Cosmochim. Acta 61, 2697-2715.
Niemi, N.A., Oskin, M., Burbank, D.W., Heimsath, A.M., Gabet, E.J., 2005. Effects of bedrock landslides on cosmogenically-determined erosion rates. Earth Planet. Sci. Lett., 237, 480-498.
Nishiizumi, K., Imamura, M., Caffee, M.W., Southon, J.R., Finkel, R.C., McAninch, J., 2007. Absolute calibration of ^{10}Be AMS standards. Nucl. Instr. Meth. Phys. Res. B 258, 403-413.
Owen, L.A., Finkel, R.C., Barnard, P.L., Ma, H.Z., Asahi, K., Caffee, M.W., Derbyshire, E., 2005. Climatic and topographic controls on the style and timing of Late Quaternary glaciation throughout Tibet and the Himalaya defined by ^{10}Be cosmogenic radionuclide surface exposure dating. Quat. Sci. Rev. 24, 1391-1411.
Owen, L.A., Caffee, M.W., Finkel, R.C., Seong, Y.B., 2008. Quaternary glaciation of the Himalayan–Tibetan orogen. J. Quat. Sci. 23, 513-531.
Pan, Y., Kidd, W.S.F., 1992. Nyainqentanglha shear zone: A late Miocene extensional detachment in the southern Tibetan Plateau. Geology 20, 775-778.
Riebe, C.S., Kirchner, J.W., Granger, D.E., 2001. Quantifying quartz enrichment and its consequences for cosmogenic measurements of erosion rates from alluvial sediment and regolith. Geomorphology 40, 15-19.
Riebe, C.S., Kirchner, J.W., Finkel, R.C., 2003. Long-term rates of chemical weathering and physical erosion from cosmogenic nuclides and geochemical mass balance. Geochim. Cosmochim. Acta 67, 4411-4427.
Royden, L.H., Burchfiel, B.C., King, R.W., Wang, E., Chen, Z., Shen, F., Liu, Y., 1997. Surface deformation and lower crustal flow in eastern Tibet. Science 276, 788-790.
Schäfer, J.M., Tschudi, S., Zhao, Z., Wu, X., Ivy-Ochs, S., Wieler, R., Baur, H., Kubik, P.W., Schlüchter, C., 2002. The limited influence of glaciations in Tibet on global climate over the past 170 000 yr. Earth Planet. Sci. Lett. 194, 287-297.
Schoenbohm, L.M., Burchfiel, B.C., Chen, L., 2006. Propagation of surface uplift, lower crustal flow, and Cenozoic tectonics of the southeast margin of the Tibetan Plateau. Geology 34, 813-816.
Small, E.E., Anderson, R.S., Hancock, G.S., 1999. Estimates of the rate of regolith production using ^{10}Be and ^{26}Al from an alpine hillslope. Geomorphology 27, 131-150.
Sobel, E.R., Hilley, G.E., Strecker, M.R., 2003. Formation of internally drained contractional basins by aridity-limited bedrock incision. J. Geophys. Res. 108, 2344.
Staiger, J., Gosse, J., Toracinta, R., Oglesby, B., Fastook, J., Johnson, J.V., 2007. Atmospheric scaling of cosmogenic nuclide production: Climate effect. J. Geophys. Res. 112, B02205, doi:10.1029/2005JB003811.
Stone, J.O., 2000. Air pressure and cosmogenic isotope production. J. Geophys. Res. 105, 23,753-23,759.
Strobl, M., Hetzel, R., Ding, L., Zhang, L., Hampel, A., 2010. Preservation of a large-scale bedrock peneplain suggests long-term landscape stability in southern Tibet. Zeitschrift für Geomorphologie 54, 453-466.
Tapponnier, P., Xu, Z., Roger, F., Meyer, B., Arnaud, N., Wittlinger, G., Yang, J., 2001. Oblique stepwise rise and growth of the Tibet Plateau. Science 294, 1671-1677.
Thompson, L.G., Yao, T., Davis, M.E., Henderson, K.A., Mosley-Thompson, E., Lin, P.N.,

Beer, J., Synal, H.A., Cole-Dai, J., Bolzan, J.F., 1997. Tropical climate instability: The last glacial cycle from a Qinghai-Tibetan ice core. Science 276, 1821-1825.

van der Beek, P., Van Melle, J., Guillot, S., Pêcher, A., Reiners, P.W., Nicolescu, S., Latif, M., 2009. Eocene Tibetan plateau remnants preserved in the northwest Himalaya. Nature Geoscience 2, 364-368.

Vermeesch, P., 2007. CosmoCalc: An Excel add-in for cosmogenic nuclide calculations. Geochem. Geophys. Geosyst. 8, Q08003, doi:10.1029/2006GC001530.

von Blanckenburg, F., 2006. The control mechanisms of erosion and weathering at basin scale from cosmogenic nuclides in river sediment. Earth Planet. Sci. Lett. 242, 224-239.

Wang, R.L., Scarpitta, S.C., Zhang, S.C., Zheng, M.P., 2002. Later Pleistocene/Holocene climate conditions of Qinghai-Xizhang Plateau (Tibet) based on carbon and oxygen stable isotopes of Zabuye Lake sediments. Earth Planet. Sci. Lett. 203, 461-477.

Wu, Z., Barosh, P.J., Wu, Z.H., Hu, D.G., Xun, Z., Ye, P.S., 2008. Vast early Miocene lakes of the central Tibetan Plateau. Geol. Soc. Am. Bull. 120, 1326-1337.

Xu, R.H., Schärer, U., Allègre, C.J., 1985. Magmatism and metamorphism in the Lhasa Block (Tibet) - a geochronological study. J. Geol. 93, 41-57.

Yin, A., Harrison, T.M., 2000. Geologic evolution of the Himalayan-Tibetan orogen. Ann. Rev. Earth Planet. Sci. 28, 211-280.

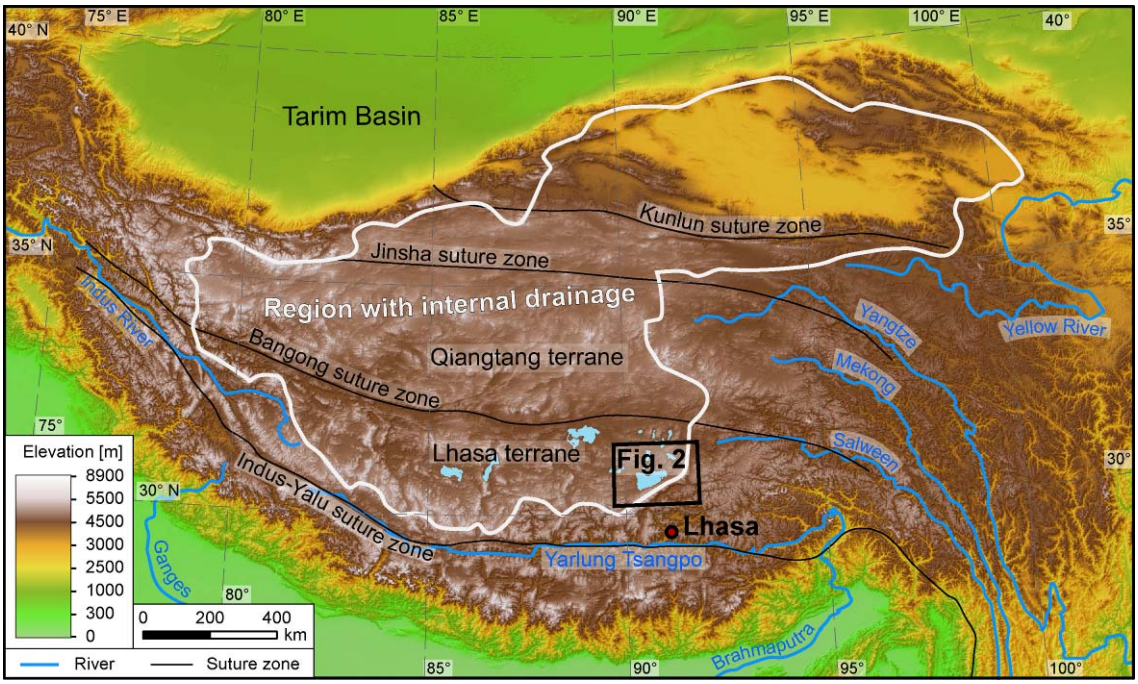

Fig. 1: Digital elevation model (90 m SRTM data) of the Tibetan Plateau and surrounding regions. Major rivers are shown in blue and the main suture zones as black lines (after DeCelles et al., 2002; Ding et al., 2003). The white line delineates the area of internal drainage (modified from Liu-Zeng et al., 2008).

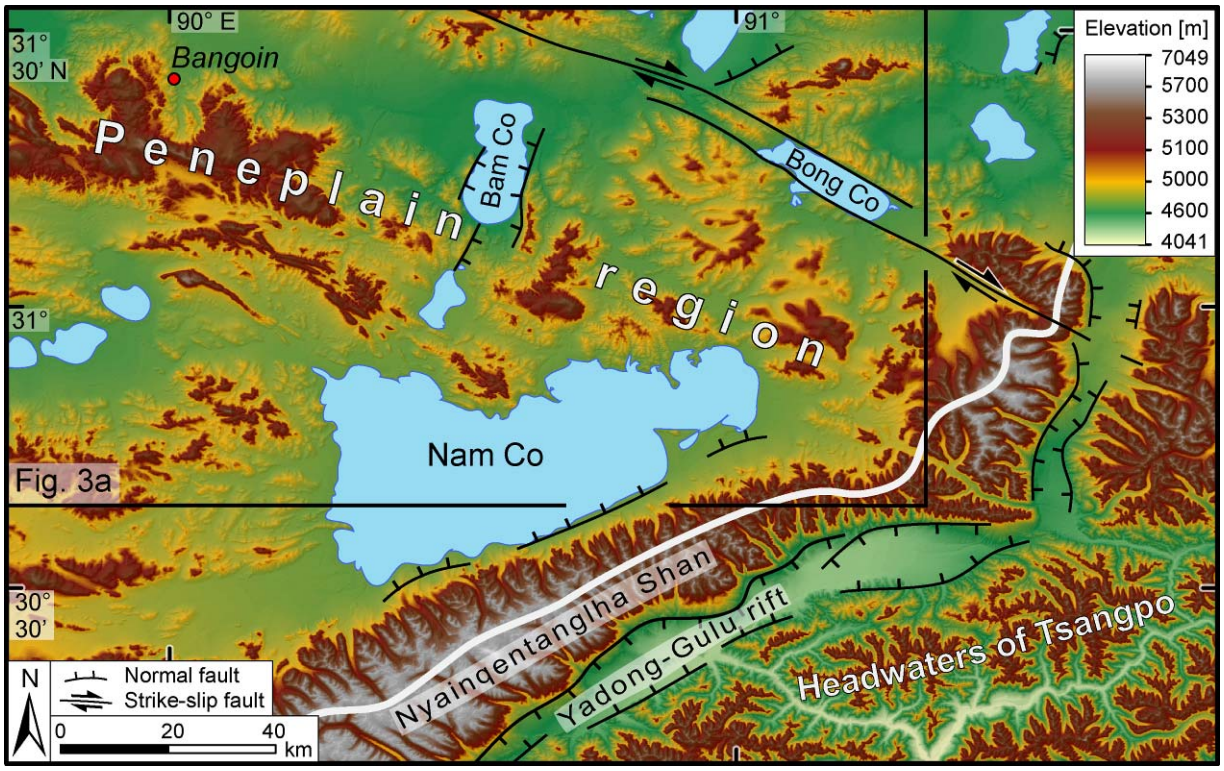

Fig. 2: Digital elevation model of the Nam Co region with lakes and active faults (from Armijo et al., 1989). The high mountains of the Nyainqentanglha Shan (Chinese: "Shan" = mountain) separate the rugged morphology in the southeast from the smooth topography in the northwest. Most of the lakes are situated in the hanging wall of normal faults except Bong Co, which occupies a pull-apart basin. The flat surface of the bedrock peneplain north of Nam Co is at an elevation of ~5300 m and appears in brownish colors. The white line delineates the boundary between the area of internal drainage and the catchment of the Tsangpo river.

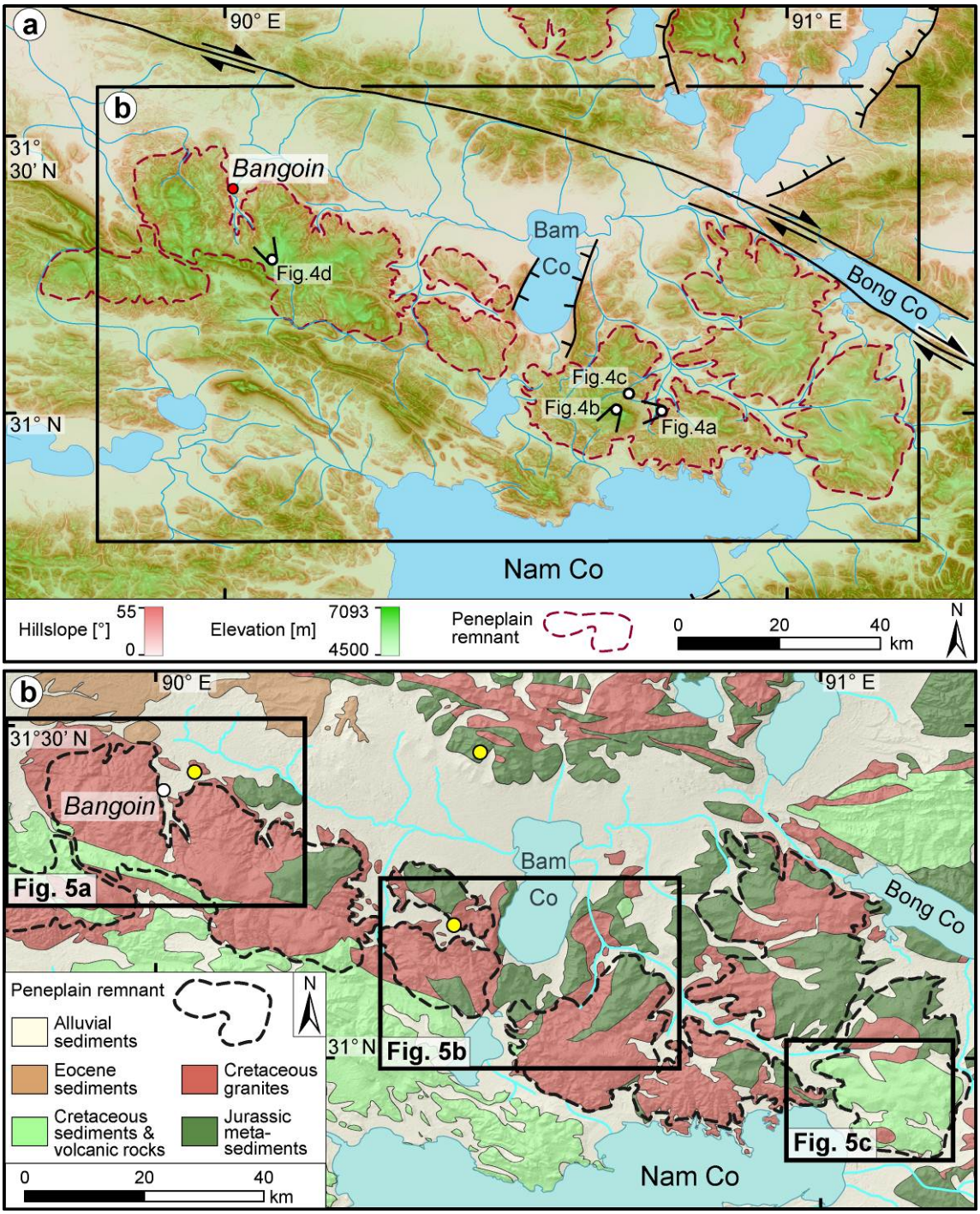

Fig. 3: (a) Map of the study area illustrating the spatial variations in elevation (green) and hillslope angle (red). The subhorizontal peneplain remnants appear in greenish color and are outlined with a purple dashed line. Note that slope angles in the valleys dissecting the peneplain increase towards lower elevation as shown by the increasing intensity of the red color towards lower elevation. Dark red to brownish colors indicate mountain ranges outside the peneplain area. The location and view direction of four field photographs shown in Fig. 4 is also indicated. **(b)** Geological map of the region north of Nam Co with a shaded relief image as background. The map has been simplified from Chinese geological maps with a scale of 1: 200,000 and our own field observations. The best preserved parts of the peneplain are located in Cretaceous granitoids and Jurassic metasediments. The locations of three samples analyzed for ^{10}Be by Lal et al. (2003) are shown as yellow dots.

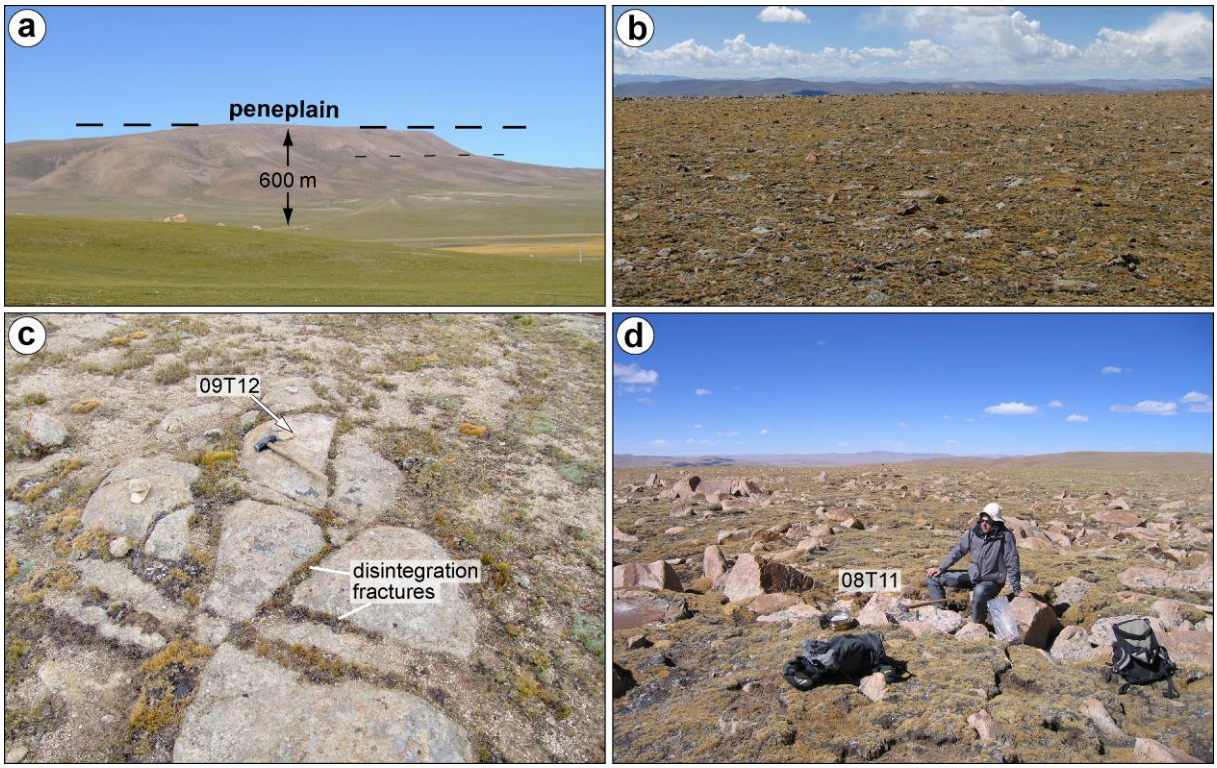

Fig. 4: Field images illustrating the topography of the bedrock peneplain. The locations and view directions of the pictures are shown in Fig. 3a. **(a)** Westward view to a well preserved remnant of the flat bedrock peneplain at an elevation of ~5400 m. The thin dashed line indicates the poorly preserved remnant of a lower bedrock surface, which has been largely eroded by continuing valley incision. **(b)** Detailed view over the flat surface of the peneplain remnant shown in (a). The surface is covered by a block field and underlain by Cretaceous granite. A grus sample (09T5) taken from the thin soil between the granitic blocks yielded a denudation rate of ~8.0 m Ma^{-1}. View is to the SSW. **(c)** Flat bedrock exposure with disintegration fractures at an elevation of ~5100 m. At this location we took a bedrock specimen (09T12) and a grus sample (09T13), which yielded similar denudation rates of ~5.6 and ~7.8 m Ma^{-1}. **(d)** Block field on the peneplain southeast of Bangoin at an elevation of ~5350 m. A bedrock sample (08T11) taken from the block with the hammer in front of Marcus Strobl gave a high apparent denudation rate of ~20.2 m Ma^{-1}, whereas a grus sample from this site (08T12) yielded a rate of only ~6.8 m Ma^{-1}, which is considered as representative for the long-term denudation of the surface.

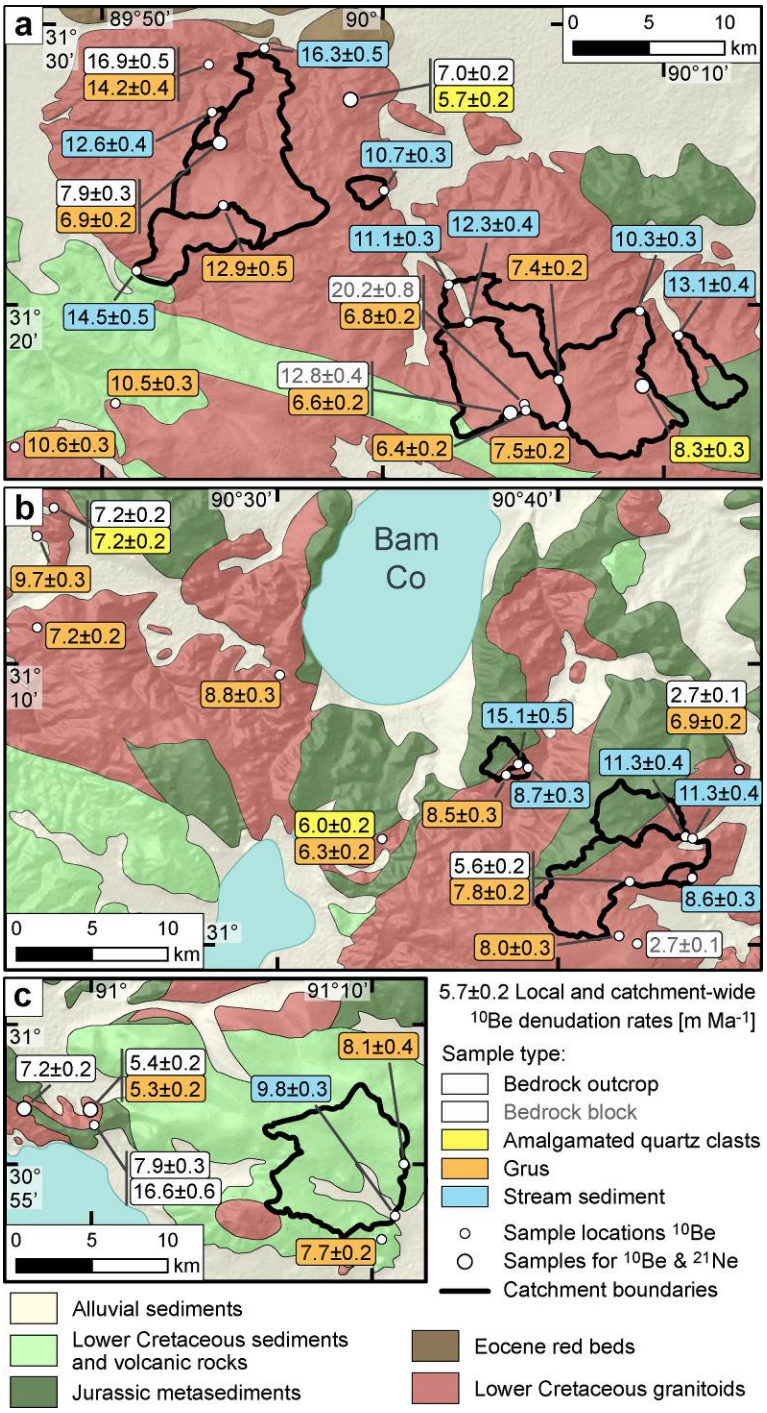

Fig. 5 (a-c): All ^{10}Be denudation rates obtained in this study plotted on three geological maps with shaded relief images as background. The stated errors represent the internal uncertainties (1σ) that are relevant to compare the results from different samples (external uncertainties are given in Tables 1 and 2). Local denudation rates, which were derived from four different types of samples, are nearly always lower than spatially integrated denudation rates for nearby catchments, except for a few bedrock samples. Note that the local denudation rates are independent from the sample elevation. The positions of the three maps are indicated in Fig. 3b.

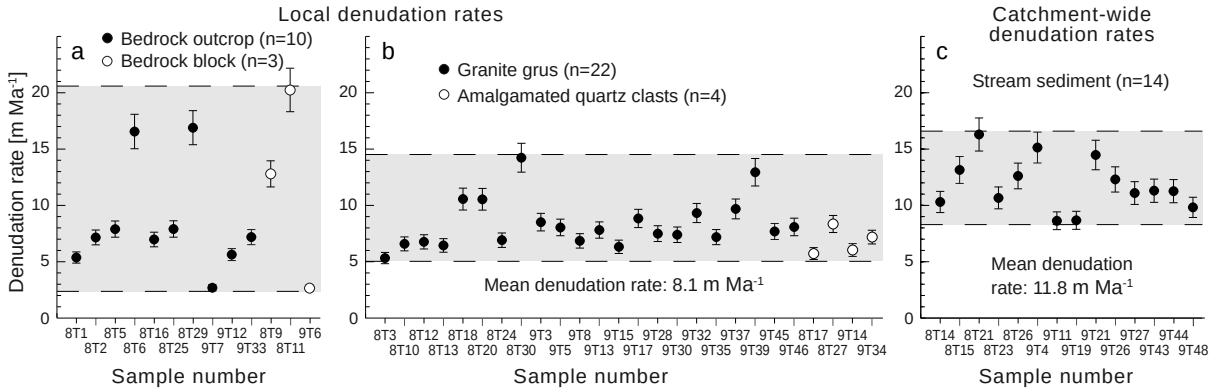

Fig. 6: Comparison of denudation rates derived from different sample types. Error bars denote external 1σ errors. The errors of points without visible error bars are smaller than the dot. **(a)** Bedrock outcrop and bedrock block samples show a large scatter of denudation rates and may overestimate the long-term rate. **(b)** Denudation rates derived from granite grus and quartz clasts are more evenly distributed and are considered to be more representative. **(c)** Small differences between catchment-wide denudation rates and those obtained from grus and quartz clasts suggest a slow process that has been active for millions of years.

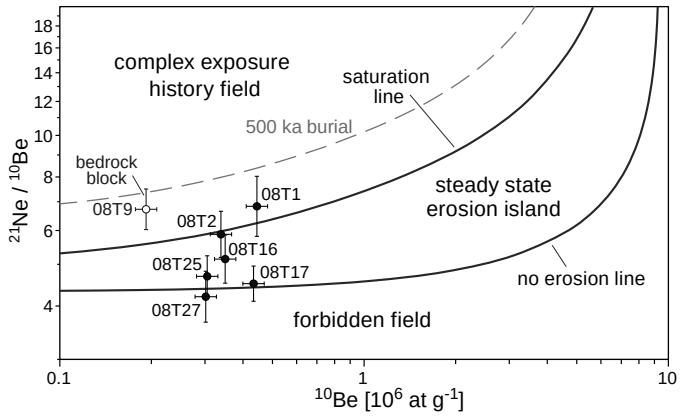

Fig. 7: Erosion island plot for the subset of seven samples in which both ^{10}Be and ^{21}Ne were analyzed. The plot was generated with CosmoCalc, version 1.7 (Vermeesch, 2007), using the time-invariant scaling scheme of Stone (2000) and the following parameters: a total production rate of 4.66 at g^{-1} a^{-1} for ^{10}Be and 20.1 at g^{-1} a^{-1} for ^{21}Ne, a contribution of 2.1% from slow muons and 1.9% from fast muons to ^{10}Be production and of 3.6% from fast muons to ^{21}Ne production (cf. Goethals et al., 2009b and references therein), a ^{10}Be decay constant of 5.00×10^{-7} a^{-1} (corresponding to a half-life of 1.387 Ma), the preset production rate mechanisms of CosmoCalc with three exponentials, and the default values for the attenuation lengths. Error bars represent 2σ uncertainties.

Table 1: ^{10}Be concentrations, production rates, and local denudation rates derived from different sample types in the Nam Co region, southern Tibet.

Sample type and number	Latitude WGS 84 (°N)	Longitude (°E)	Elevation (m)	Sample thickness (cm)	^{10}Be conc. [a] (10^4 at g^{-1})	Production rate [b] spallation (at g^{-1} a^{-1})	muons (at g^{-1} a^{-1})	Denudation rate [c] (m Ma^{-1})	Internal 1σ error (m Ma^{-1})	External 1σ error (m Ma^{-1})	Time scale [d] (ka)
Bedrock outcrop											
08T1	30.9398	91.0018	4911	4.0	814 ± 24	77.29	0.734	5.37	±0.17	±0.52	112
08T2	30.9495	90.9603	5013	4.0	650 ± 20	80.96	0.752	7.15	±0.23	±0.69	84
08T5	30.9491	90.9994	4784	3.0	539 ± 16	72.93	0.716	7.89	±0.24	±0.75	76
08T6	30.9490	90.9995	4783	2.5	265 ± 10	72.89	0.719	16.55	±0.63	±1.59	36
08T16	31.4548	89.9809	4916	3.5	651 ± 20	78.85	0.738	6.97	±0.22	±0.68	86
08T25	31.4293	89.9033	5203	5.0	647 ± 19	89.55	0.783	7.90	±0.25	±0.76	76
08T29	31.4758	89.8970	4823	5.0	263.7 ± 7.9	75.62	0.716	16.89	±0.52	±1.58	36
09T7	31.1035	90.7748	4846	3.5	1502 ± 45	75.42	0.725	2.69	±0.09	±0.28	223
09T12	31.0370	90.7095	5099	3.5	852 ± 26	84.37	0.770	5.63	±0.24	±0.55	107
09T33	31.2580	90.3680	4838	5.0	625 ± 19	75.54	0.742	7.18	±0.23	±0.70	78
Bedrock block											
08T9	31.2690	90.0759	5306	4.5	424 ± 13	93.14	0.803	12.79	±0.39	±1.21	47
08T11	31.2741	90.0842	5351	3.0	280 ± 11	94.99	0.819	20.23	±0.82	±1.98	30
09T6	31.0001	90.7142	5395	3.0	1933 ± 58	95.91	0.827	2.65	±0.09	±0.28	226
Amalgamated quartz clasts											
08T17	31.4548	89.9809	4916	1.0	807 ± 24	78.85	0.754	5.67	±0.18	±0.55	106
08T27	31.2848	90.1544	5070	1.0	600 ± 18	84.00	0.781	8.28	±0.26	±0.79	72
09T14	31.0625	90.5625	4896	1.0	751 ± 23	77.05	0.752	6.04	±0.19	±0.59	99
09T34	31.2592	90.3673	4817	1.0	669 ± 20	74.82	0.735	7.18	±0.21	±0.64	91
Grus [e]											
08T3	30.9398	91.0020	4910	-	848 ± 25	77.25	0.754	5.32	±0.17	±0.52	113
08T10	31.2690	90.0759	5306	-	832 ± 25	93.14	0.829	6.58	±0.21	±0.64	91
08T12	31.2741	90.0842	5351	-	827 ± 25	94.99	0.838	6.76	±0.21	±0.66	89
08T13	31.2703	90.0852	5358	-	868 ± 26	95.26	0.840	6.44	±0.20	±0.62	93
08T18	31.2487	89.7821	5260	-	519 ± 15	91.19	0.820	10.56	±0.33	±1.01	57
08T20	31.2747	89.8416	5109	-	488 ± 15	85.42	0.792	10.54	±0.33	±1.00	57
08T24	31.4293	89.9033	5203	-	765 ± 23	89.55	0.810	6.91	±0.22	±0.67	87
08T30	31.4758	89.8970	4823	-	324.3 ± 9.7	75.62	0.740	14.23	±0.44	±1.34	42
09T3	31.1004	90.6361	5095	-	592 ± 18	84.40	0.789	8.51	±0.27	±0.81	71
09T5	31.0048	90.7032	5436	-	721 ± 22	97.62	0.854	8.04	±0.25	±0.77	75
09T8	31.1035	90.7748	4845	-	652 ± 19	75.38	0.743	6.85	±0.21	±0.67	87
09T13	31.0370	90.7095	5099	-	642 ± 19	84.37	0.789	7.81	±0.24	±0.75	77
09T15	31.0625	90.5625	4896	-	720 ± 22	77.05	0.752	6.32	±0.20	±0.61	95

09T17	31.1599	90.5018	4782	-	498 ± 15	73.36	0.732	8.84	±0.28	±0.84	68
09T28	31.2614	90.1071	5434	-	776 ± 23	98.39	0.854	7.49	±0.24	±0.73	80
09T30	31.2885	90.1044	5333	-	755 ± 23	94.30	0.835	7.39	±0.23	±0.72	81
09T32	31.2580	90.3680	4838	-	488 ± 15	75.54	0.742	9.32	±0.29	±0.89	64
09T35	31.1880	90.3573	4998	-	669 ± 20	81.05	0.771	7.18	±0.23	±0.70	84
09T37	31.2425	90.3574	4658	-	433 ± 13	69.44	0.710	9.68	±0.30	±0.92	62
09T39	31.3921	89.9053	5418	-	458 ± 18	98.17	0.852	12.94	±0.52	±1.27	46
09T45	30.8719	91.1727	5047	-	635 ± 19	82.03	0.780	7.68	±0.24	±0.74	78
09T46	30.9166	91.1859	5215	-	651 ± 27	88.50	0.811	8.08	±0.35	±0.81	74

[a] Blank-corrected ^{10}Be concentrations. Propagated analytical errors (1σ) include the error based on counting statistics and the error of the blank correction. ^{10}Be concentrations were measured at ETH Zurich and are normalized to the secondary standard S2007N with a nominal ^{10}Be/^{9}Be ratio of 28.1 x 10^{-12} (Kubik and Christl, 2010).

[b] The reported ^{10}Be production rates were calculated with the CRONUS-Earth ^{10}Be - ^{26}Al calculator, version 2.2 (Balco et al., 2008; http://hess.ess.washington.edu), using the time-invariant production rate scaling model of Lal (1991) - Stone (2000). The sea level and high latitude ^{10}Be production rate due to neutron spallation is 4.49 ± 0.39 at g^{-1} yr^{-1} (updated constants file version 2.2.1 of online calculator), with an additional contribution of 2.1% by negative muon capture and 1.9% by fast muons (Heisinger et al., 2002). An assumed rock density of 2.7 g cm^{-3} andthe sample thickness specified in the table is taken into account. Topographic shielding of all samples is negligible.

[c] Denudation rates were calculated with the CRONUS-Earth ^{10}Be - ^{26}Al calculator, version 2.2 (Balco et al., 2008; http://hess.ess.washington.edu). Internal uncertainties include errors from the counting statistics and the blank correction, whereas external uncertainties also include the systematic uncertainty of the sea level high latitude production rate. Note that the 2.7 % error associated with the ^{10}Be/^{9}Be ratio of the standard S2007N is also included in the external uncertainty.

[d] The time over which the denudation rate integrates is calculated by dividing the absorption depth scale of 60 cm by the denudation rate.

[e] For determining local denudation rates from grus samples, we used the 0.5–2 mm grain size fraction.

Table 2: ^{10}Be concentrations, production rates, and catchment-wide denudation rates derived from stream sediment samples in the Nam Co region, southern Tibet.

Sample type and number	Latitude WGS 84 (°N)	Longitude WGS 84 (°E)	Elevation of sample (m)	Mean catchment elevation (m)	Topographic shielding factor	^{10}Be conc. [a] (10^4 at g^{-1})	Production rate [b] (spallation) (at g^{-1} a^{-1})	Production rate [b] (muons) (at g^{-1} a^{-1})	Denudation rate [c] (m Ma^{-1})	Internal 1σ error (m Ma^{-1})	External 1σ error (m Ma^{-1})	Time scale [d] (ka)
Stream sediment [e]												
08T14	31.3293	90.1526	4714	5201	0.9974	518 ± 16	88.93	0.810	10.30	±0.32	±0.98	58
08T15	31.3147	90.1759	4822	5171	0.9984	405 ± 12	87.80	0.804	13.14	±0.41	±1.24	46
08T21	31.4854	89.9299	4783	5070	0.9963	315.6 ± 9.5	84.30	0.785	16.29	±0.50	±1.53	37
08T23	31.4009	90.0009	4734	4921	0.9954	445 ± 13	78.52	0.758	10.66	±0.33	±1.01	56
08T26	31.4475	89.8987	4893	5054	0.9973	402 ± 12	83.66	0.782	12.61	±0.39	±1.19	48
09T4	31.1069	90.6435	4850	5018	0.9945	326.8 ± 9.8	81.11	0.775	15.13	±0.47	±1.43	40
09T11	31.0392	90.7468	4801	4952	0.9969	546 ± 16	78.74	0.762	8.63	±0.27	±0.82	70
09T19	31.1048	90.6493	4808	4984	0.9948	551 ± 17	79.89	0.768	8.67	±0.27	±0.83	70
09T21	31.3534	89.8542	4783	5193	0.9981	372 ± 11	88.74	0.808	14.47	±0.45	±1.37	41
09T26	31.3224	90.0513	4804	5202	0.9975	437 ± 13	88.96	0.810	12.30	±0.38	±1.17	49
09T27	31.3450	90.0392	4776	5169	0.9970	476 ± 14	87.70	0.804	11.09	±0.34	±1.05	54
09T43	31.0638	90.7427	4792	5055	0.9978	441 ± 13	82.62	0.781	11.30	±0.35	±1.07	53
09T44	31.0626	90.7469	4781	5060	0.9979	444 ± 13	82.81	0.782	11.26	±0.35	±1.07	53
09T48	30.8857	91.1809	4853	5055	0.9994	504 ± 15	82.31	0.781	9.82	±0.31	±0.94	61

[a] Blank-corrected ^{10}Be concentrations. Propagated analytical errors (1σ) include the error based on counting statistics and the error of the blank correction. ^{10}Be concentrations were measured at ETH Zurich and are normalized to the secondary standard S2007N with a nominal ^{10}Be/^{9}Be ratio of 28.1 x 10^{-12} (Kubik and Christl, 2010).

[b] The reported ^{10}Be production rates were calculated with the CRONUS-Earth ^{10}Be - ^{26}Al calculator, version 2.2 (Balco et al., 2008; http://hess.ess.washington.edu), using the time-invariant production rate scaling model of Lal (1991) - Stone (2000). The sea level and high latitude ^{10}Be production rate due to neutron spallation is 4.49 ± 0.39 at g^{-1} yr^{-1} (updated constants file version 2.2.1 of online calculator), with an additional contribution of 2.1% by negative muon capture and 1.9% by fast muons (Heisinger et al., 2002). The rock density was considered with 2.7 g cm^{-3}. For the topographic shielding correction, we calculated a shielding factor for each catchment by using 30 m Aster Digital Elevation Models and the Matlab script of Greg Balco (http://depts.washington.edu/cosmolab/shielding.m).

[c] Denudation rates were calculated with the CRONUS-Earth ^{10}Be - ^{26}Al calculator, version 2.2 (Balco et al., 2008; http://hess.ess.washington.edu). Internal uncertainties include errors from the counting statistics and the blank correction, whereas external uncertainties also include the systematic uncertainty of the sea level high latitude production rate. Note that the 2.7 % error associated with the ^{10}Be/^{9}Be ratio of the standard S2007N is also included in the external uncertainty. For the calculation of catchment-wide denudation rates we used the mean elevation of the respective catchments.

[d] The time over which the denudation rate integrates is calculated by dividing the absorption depth scale of 60 cm by the denudation rate.

[e] For determining catchment-wide denudation rates from stream sediment samples, we used the 0.25–0.5 mm grain size fraction.

Table 3: Results of Ne analyses of quartz separates from samples from the Nam Co region, southern Tibet.

Sample	Temp. (°C)	^{20}Ne (10^{-12} cm^3 STP/g)	$^{22}Ne/^{20}Ne$	$^{21}Ne/^{20}Ne$	$^{21}Ne_{ex}$ [a] (10^6 at/g)
Bedrock outcrop					
08T1	400	40.3 ± 3.2	0.1535 ± 0.0024	0.0484 ± 0.0010	49.1 ± 3.8
	600	72.4 ± 5.7	0.1225 ± 0.0016	0.00892 ± 0.00025	11.4 ± 1.0
	800	61.0 ± 4.9	0.1181 ± 0.0025	0.00434 ± 0.00018	2.08 ± 0.34
	1200	13.1 ± 1.3	0.464 ± 0.017	0.01322 ± 0.00077	3.57 ± 0.35
	Total	**186.8 ± 8.3**	**0.1517 ± 0.0030**	**0.01624 ± 0.00072**	**55.8 [b] ± 7.8**
	crusher	300 ± 15	0.10183 ± 0.00078	0.003063 ± 0.000059	–
08T2	400	38.0 ± 2.2	0.1254 ± 0.0026	0.02690 ± 0.00062	24.4 ± 1.5
	600	110.7 ± 7.1	0.1054 ± 0.0013	0.00722 ± 0.00014	12.52 ± 0.91
	800	331 ± 21	0.10114 ± 0.00033	0.003166 ± 0.000042	1.33 ± 0.54
	1200	92.7 ± 6.0	0.1026 ± 0.0011	0.00343 ± 0.00011	1.01 ± 0.30
	Total	**572 ± 23**	**0.10381 ± 0.00042**	**0.00557 ± 0.00014**	**38.3 ± 1.8**
	crusher	683 ± 49	0.10136 ± 0.00034	0.003016 ± 0.000043	–
08T16	400	22.2 ± 1.5	0.1550 ± 0.0033	0.0411 ± 0.0012	22.6 ± 1.5
	600	38.2 ± 2.3	0.1114 ± 0.0011	0.01320 ± 0.00039	10.38 ± 0.74
	800	34.0 ± 2.2	0.1018 ± 0.0015	0.00382 ± 0.00017	0.66 ± 0.24
	1200	7.53 ± 0.68	0.1024 ± 0.0026	0.0185 ± 0.0016	3.13 ± 0.33
	Total	**101.9 ± 3.6**	**0.1170 ± 0.0012**	**0.01654 ± 0.00056**	**33.6 ± 1.7**
	crusher	41.6 ± 3.0	0.10318 ± 0.00089	0.00308 ± 0.00020	–
08T25	400	33.6 ± 2.7	0.1385 ± 0.0029	0.03474 ± 0.00086	28.5 ± 2.3
	600	14.5 ± 1.3	0.1084 ± 0.0047	0.00779 ± 0.00068	1.85 ± 0.30
	800	8.1 ± 1.1	0.1035 ± 0.0063	0.00326 ± 0.00038	0.048 +0.086/-0.048
	1200	3.69 ± 0.70	0.1018 ± 0.0071	0.0161 ± 0.0029	1.29 ± 0.23
	Total	**59.9 ± 3.3**	**0.1242 ± 0.0024**	**0.02281 ± 0.00091**	**30.4 ± 2.3**
	crusher	37.2 ± 2.0	0.1029 ± 0.0016	0.00302 ± 0.00012	–
Bedrock block					
08T9	400	72.9 ± 5.7	0.11328 ± 0.00094	0.01529 ± 0.00035	23.9 ± 2.0
	600	81.2 ± 6.3	0.1035 ± 0.0012	0.00485 ± 0.00018	3.81 ± 0.52
	800	71.4 ± 5.7	0.1029 ± 0.0018	0.00356 ± 0.00019	0.88 ± 0.41
	1200	2.43 ± 0.66	0.115 ± 0.010	0.0371 ± 0.0092	2.21 ± 0.33
	Total	**228 ± 10**	**0.10656 ± 0.00080**	**0.00813 ± 0.00030**	**28.6 ± 2.1**
	crusher	157.5 ± 8.1	0.10171 ± 0.00077	0.003097 ± 0.000098	–
Amalgamated quartz clasts					
08T17	400	52.4 ± 2.8	0.11256 ± 0.00089	0.01286 ± 0.00033	13.88 ± 0.87
	600	165.8 ± 8.6	0.1089 ± 0.0012	0.00785 ± 0.00015	21.6 ± 1.4
	800	185.5 ± 9.8	0.10284 ± 0.00081	0.003204 ± 0.000050	1.02 ± 0.61
	1200	8.92 ± 0.70	0.1078 ± 0.0029	0.00308 ± 0.00067	0.02 +0.16/-0.02
	Total	**413 ± 13**	**0.10662 ± 0.00063**	**0.00629 ± 0.00012**	**36.5 ± 1.8**
	crusher	178 ± 13	0.10196 ± 0.00049	0.00300 ± 0.00011	–
08T27	400	31.5 ± 2.0	0.1280 ± 0.0015	0.02640 ± 0.00056	19.7 ± 1.2
	600	106.9 ± 6.3	0.1035 ± 0.0015	0.00491 ± 0.00015	5.28 ± 0.60
	800	115.7 ± 6.9	0.10159 ± 0.00097	0.00316 ± 0.00013	0.30 +0.51/-0.30
	1200	14.1 ± 1.0	0.1052 ± 0.0027	0.00364 ± 0.00019	0.214 ± 0.081
	Total	**268.2 ± 9.6**	**0.10564 ± 0.00079**	**0.00661 ± 0.00021**	**25.3 ± 1.4**
	crusher	129.0 ± 9.3	0.10208 ± 0.00093	0.003064 ± 0.000099	–

Error limits are 2σ.

[a] Excess ^{21}Ne relative to the trapped Ne composition as determined by crushing extractions (see last line for each sample). Totals show estimated concentrations of cosmogenic ^{21}Ne, calculated based on the excesses in the 400-800°C steps (see text).

[b] For sample 08T1 only (50±50) % of the ^{21}Ne excesses in the 600°C and 800°C steps was added to the 400°C excess to obtain total cosmogenic Ne, as the three-isotope systematics (Fig. S1) indicates a contribution by nucleogenic Ne at higher temperatures.

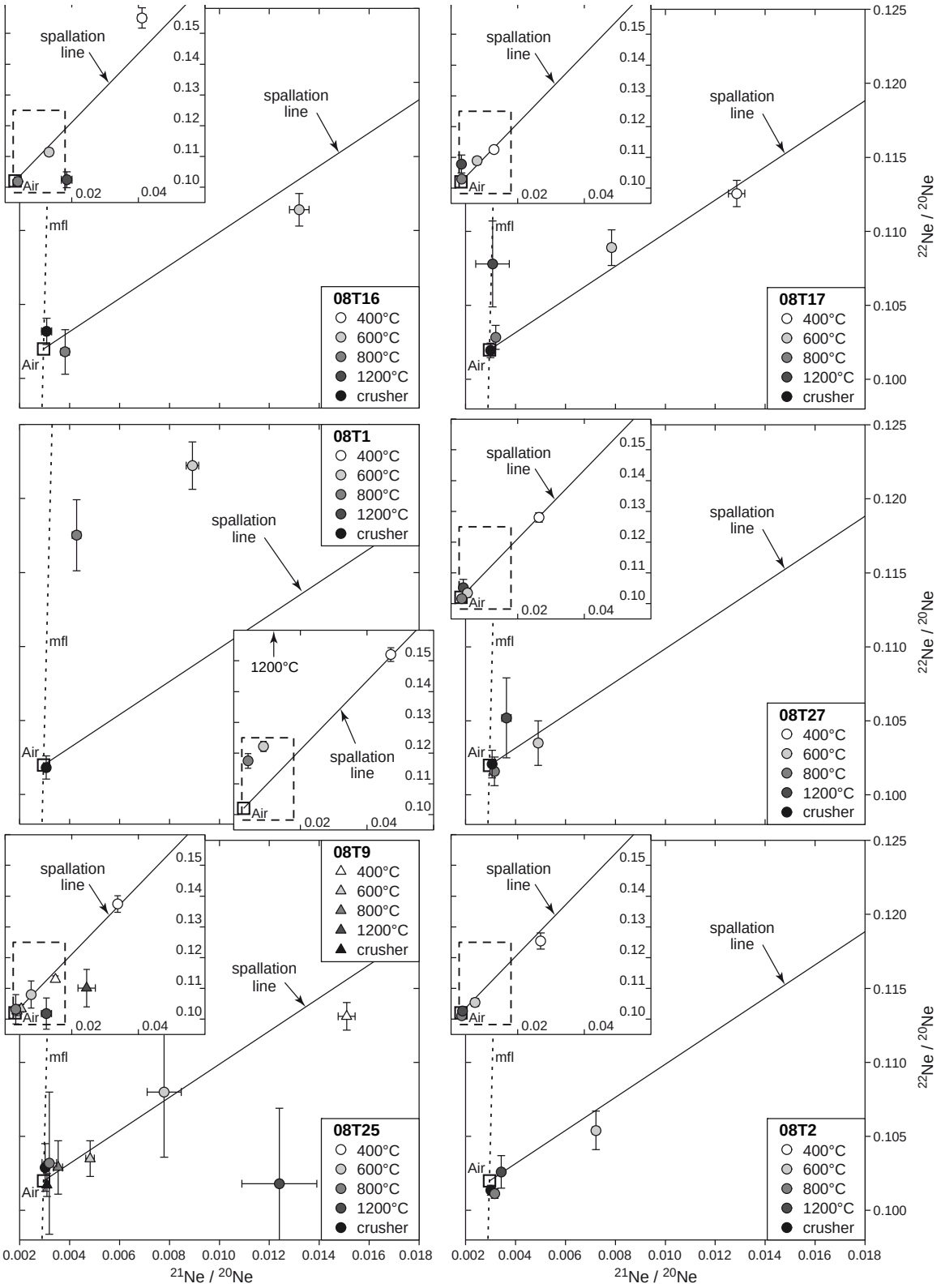

Fig. A.1: Ne three-isotope diagrams for seven quartz samples analyzed (note that the plot in the lower left contains the data of two samples). Circles represent the neon isotopic compositions of gas released at 400, 600, 800, and 1200 °C, whereas the open squares represent the neon composition of air. Gas extracted by crushing (black circles) has a neon isotopic composition that is similar to air. The spallation line represents the mixing line between atmospheric and cosmogenic Ne for quartz (Niedermann et al., 1993). The dashed line corresponds to mass-fractionated atmospheric Ne (mfl).